INSTRUMENTATION

THE N3 VAULT--A GENERAL PURPOSE USER STATION

D.P. Sanderson

The completion of Phase II of the laboratory's construction will provide five stations for nuclear physics experiments. The third vault on the north side is designed as a general purpose stations for a wide range of experiments. (See Fig. 1.)

The main feature of the vault is the 92" Scattering Chamber, previously installed in the interim vault. The cramped quarters made setting up a complicated experiment with large amounts of electronics in the vault difficult. The new spacious environs of the N3 vault will make such setups much easier.

The scattering chamber[1] is a large 234 cm diameter right circular cylinder on its side. Two cantilevered rails, 74 cm below beam height, support a removable detector/target mounting system. A square fixed baseplate (152.4 X 152.4 cm) is mounted 71.4 cm below the beam axis. Extruded aluminum rails can be attached to the baseplate for mounting fixed detector arrays.

At 58.2 cm below the beam axis, a 152.4 cm diameter turntable is mounted. A radial pattern of threaded inserts allow up to 200 kg of detectors to be mounted on the table. A radial arm, rated at 20 kg can be installed above the turntable at 46.8 cm below beam height. At the center of this assembly, a target ladder can insert up to nine of the laboratory's standard targets. All motional degrees of freedom are

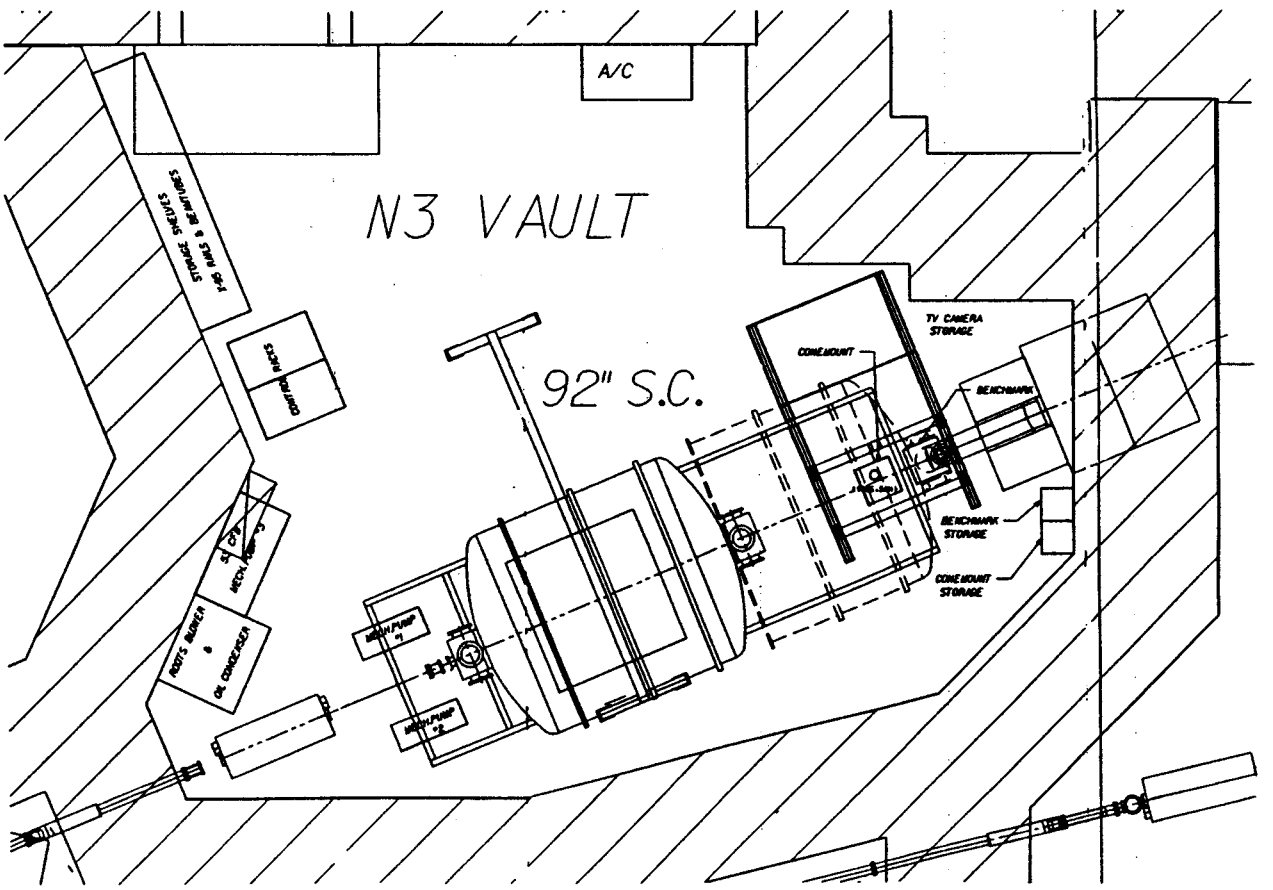

Fig. 1. The N3 Vault.

driven by high torque stepping motors with absolute encoder monitoring of position. Control is either locally, through a panel in the vault, or remotely by logging onto the control system computer.

The high vacuum system consists of two large turbo pumps and a liquid nitrogen cold trap. Pumpdown to 4×10^{-5} Torr requires approximately three hours. The vacuum system will be upgraded in late 1990 with the installation of liquid helium cryopumps. They should reduce the pumpdown time to one hour.

Detector electronics in the vault are well provided for. Camac serial and parallel highways are cabled to the chamber area. Two hundred special low noise shielded signal cables are installed on the chamber with terminations in Data-U 6. High voltage and low impedance wiring follow a noise free path back to the data-U. Crate power of up to 45 kW is available through a "clean" isolation transformer.

During the last two years of operation in the interim vault, the 92" Scattering Chamber has been extremely flexible. In some cases, a beamline was attached to the inside of the chamber to connect a user supplied scattering chamber to the main beamline. At one point, the back of the main vacuum vessel was removed and a large dipole magnet was installed at the normal target position.

In summary, the movement of the 92" Scattering Chamber to the N3 vault has created a large versatile user station with plenty of room and flexibility. Past experience in the interim vault has shown that it will be a very useful facility for years to come.

References

1. NSCL Annual Report (1987) p. 227.

THE A1200 BEAM ANALYSIS DEVICE

B.M. Sherrill, D.J. Morrissey, J.A. Nolen, Jr., C. Snow, G. Stork, and J.A. Winger

In order to provide the highest quality beams for experiments it is desirable to have a beam analysis device between the K1200 cyclotron and the experimental areas. Such a device is also suited for the production and separation of secondary beams for direct use in experiments and/or for calibrations. Similar devices exist or are under construction at other Laboratories, namely the Alpha Spectrometer[1] at GANIL, the related work with radioactive beams at LISE[2] and SPEG[3] at GANIL for secondary beam production and separation, and the large project at GSI for the SIS-18 accelerator which incorporates a fragment separator into the beamline for the production and separation of very intense secondary beams.[4]

The initial design of the NSCL analysis device, the A1200, was described in the 1987 annual report,[5] and at the Conference on Radioactive Nuclear Beams.[6] In this report we give an update on the final design, an outline of the various experiments it will be used for, and a status report on the construction.

There are three distinct operating modes for the device; parameters for each of these modes are listed in Table I. The first mode is the fully chromatic or high resolution mode, which gives maximum resolving power at the final image position of the device. The expected resolving power of 10,000 for a 1mm beam spot is based on results of orbit tracking studies been checked with the optimizing raytrace code MOTER. The high resolution mode will be useful for measuring the beam energy, the beam energy spread, and for providing a precise beam energy for experiments which require it. This mode also provides an intermediate image with half the full resolving power, which will be useful in experiments which require both a very clean beam and a narrow beam energy spread, since an energy cut can be made at this image and the final image can be used to clean up the beam, thus significantly reducing slit scattering. By placing an energy degrading system at the object position of the A1200 it will also be possible to tune the beam energy, or change energies quickly. The limit of how low in energy one can degrade is limited by energy and angular straggling, but changes of 20 to 30 percent should be easy to achieve.

TABLE I--OPERATING PARAMETERS FOR THE OPTICAL MODES OF THE A1200.

	MODE		
Parameter	High Res	Medium Res	Large Accept.
Ω(msr)	0.25	0.8	4.3
Δθ (mr)	10.	20.	54.
Δφ (mr)	10.	40.	80.
Δp (%)	0.4	3.0	3.0
max Bρ(Tm)	5.4	5.4	5.4
p/Δp	10000	3400	1300
(x/x)			
Int. Image	3.0	0.5	1.0
System End	1.0	1.0	1.0
(x/δ)			
Int. Image	15.0	1.8	1.3
System End	10.0	0.0	0.0
(cm/%)			

The second mode (shown schematically in Fig. 1) is a medium resolution, medium solid angle mode which can be used for achromatic beam transport. The resolving power is less than half that of the high resolution mode, but still allows momentum to be measured and defined up to 1 part in 3000. This mode will also be useful for measuring and defining the beam phase space.

Table II lists beam parameters which must be measured and controlled to set up this achromatic mode. In addition, the dependence of the horizontal angle on momentum must be known in order to make the beam transport achromatic;

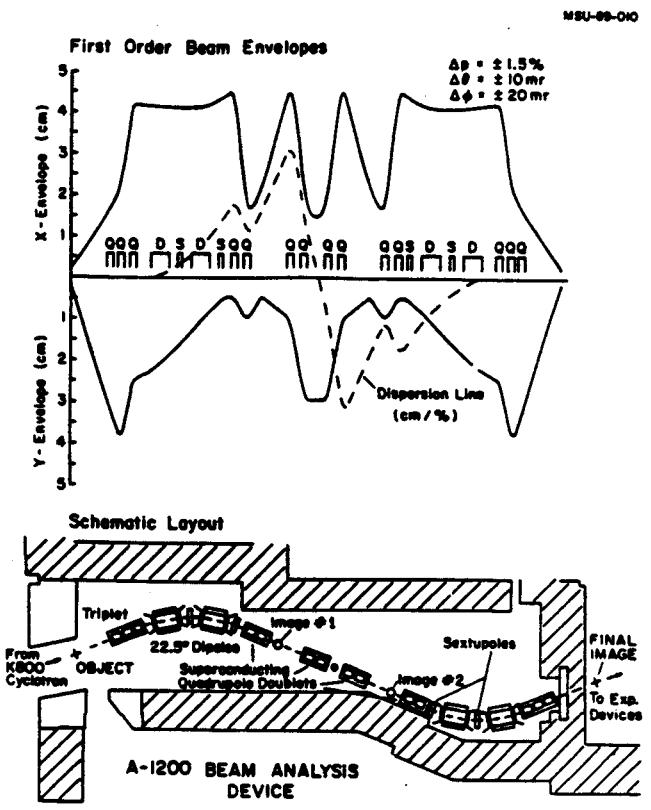

Fig. 1 Schematic layout of the medium resolution mode of the A1200 showing the beam envelopes (above), with the dispersion in cm/% shown as a dashed line. The lower part shows the floor layout. The system uses the standard NSCL beamline superconducting magnets except for two special triplets at the front and back of the device.

TABLE II--LOCATION OF MEASUREMENT AND DEFINITION OF BEAM PARAMETERS.

Parameter	Measurement Position	Definition
Δx	Focal Plane	Target
Δy	Center	Target
	Focal Plane	Center
$\Delta\theta$	Center	Divergence slits
$\Delta\phi$	Int. Images	Divergence slits
		Int. Image
p	Int. Images	Int. Image
Δp	Int. Images	Int. Image
	Focal Plane (chromatic mode)	

this can be measured by using the divergence slits to select angle, and one of the intermediate images to select a momentum, and by measuring the position shift at the final image position as a function of the distance along the beamline (back toward the last set of dipoles), the angular dispersion can be inferred. Once the angular dispersion has been measured, the A1200 can be retuned to cancel this dispersion component at the image position.

The achromatic mode will also be useful for separating secondary beams. (The physics justifications for studying secondary beams will be discussed briefly latter.) The combination of the A1200 and the RPMS will also allow very good separation of radioactive ions for decay studies with essentially zero background. Since the mass resolving power of the A1200 is proportional to the momentum resolving power,[5] there is a trade-off between larger angular acceptance and purity of the secondary beams. For many applications the purity is not critical, and a larger angular bite can be taken. The parameters in Table I for the medium acceptance mode are optimized for resolving power. The resolution has been checked with MOTER.

Using the calculated acceptance of the device, production cross sections taken from Suemmerer and Morrissey,[7] and assuming 1 pnA of primary beam intensity, Table III gives the expected secondary beam intensities. The numbers in the table were calculated with the program INTENSITY, which was written to calculate secondary beam rates and purities using profiled degraders. The program calculates the angular and momentum acceptance of the A1200 for a given fragment assuming momentum and angular spreads for the fragments from the Goldhaber model of projectile fragmentation.[8] The perpendicular momentum is taken as the Fermi momentum added in quadrature to a contribution from the nuclear reaction.[9]

The program includes multiple scattering and energy loss straggling. The energy loss is calculated with the relativistic Bethe-Block formula, and charge state distributions are taken from a parameterization of known data, which is accurate over our energy range. The examples listed in the table are meant to give an idea of the order of magnitude of secondary beam intensities which will be available. In most cases primary beam intensities of up to 100 pnA can be used, in which case secondary beam rates would exceed the numbers in the table by a factor of 100.

The third A1200 mode, the large acceptance mode, is the extreme in the trade-off between solid angle and resolution. In this mode the target is placed at the front of the first triplet, the triplet having been added to the design, instead of the doublet originally planned, to keep the angular acceptance symmetric in the large acceptance mode. This mode will be used for transmission of the maximum amount of secondary products, and yields an increase of up to 5x that of the medium acceptance mode. By placing the image position effectively beyond the true image, the beamlines for the rest of the facility can accept this larger transmission. Hence, essentially the full separated beam can be transferred to the RPMS for radioactive decay studies. This mode is made possible by the large gradients, 30 T/m, available with the NSCL superconducting beamline quadrupoles. It should be noted that in this mode the rates given in Table III should be multiplied by an additional factor of 5, although the purity will not be as good.

There are a variety of experiments which should be possible using radioactive beams produced by the A1200. In general, one might hope that radioactive beams will increase the number of nuclear probes by a factor of 10 over the presently available (stable) beams. Reaction mechanism studies that can be pursued include elastic scattering of radioactive ions, single nucleon transfer reactions such as $p(^{11}Li,d)^{10}Li$, single and double charge exchange using radioactive beams, Coulomb excitation, and perhaps multinucleon transfers. The energy spread of the fragments can be compensated for by time-of-flight measurements of the ions relative to the cyclotron rf, or by using the A1200 in the dispersion matched mode. The single and double nucleon transfer reactions on light targets allow for the possibility of using the equivalent of radioactive targets for doing (p,d) and (p,t) reactions.

It will also be possible to continue the search for the limits of nuclear stability as has been done at GANIL.[10,11] Using the additional selectivity of the RPMS it should be possible to do decay studies with very low backgrounds on nuclei far from stability. We are also planning to study the nature of peripheral reactions in this energy range, which is not at present well understood.

The mechanical designs for the A1200 components are complete, and fabrication is underway. Beamstops which collect the primary

TABLE III--CALCULATED SECONDARY BEAM INTENSITIES.*

Beam	E_B(MeV/A)	Fragment	Target Thickness (mg/cm²)	Rate (#/s)
^{15}N	120.	^{11}Li	1300.	$1.0x10^{1}$
^{15}N	120.	^{12}Be	1300.	$1.1x10^{3}$
^{16}O	100.	^{14}O	1100.	$5.7x10^{4}$
^{58}Ni	60.	^{56}Ni	160.	$2.3x10^{4}$
^{20}Ne	120.	^{19}Ne	1500.	$5x0x10^{6}$

*Assuming 1 pnA of primary beam and the medium acceptance mode. To get the rates for the high acceptance mode one must multiply the above rates by five.

beam will be located in the first set of dipoles and a flexible slit mechanism will be located just in front of the first triplet. Provisions have been made for adding a beam energy degrader just after the production target in order to make fast beam energy changes. The drive mechanisms for the water cooled targets are based on the standard NSCL beam pot design which uses air actuated cylinders. Focal plane chambers will be located at Image #2 and the final image indicated in Fig. 1. These will have air actuated plunger mechanisms so that detectors can be easily placed in or taken out of the beam. Beam profiles will be monitored with phosphor screens for normal intensity beams or plastic scintillator screens viewed by CCD cameras and image intensifiers for weak radioactive beams.

The components of the A1200 will be controlled by computer, which should allow easy tuning of new radioactive beams. The system will also provide fast, automated measurements of beam parameters.

References

1. R. Rebmeister, G. Gaudiot, P. Wagner, GANIL Report CRN/PN 83-16.
2. D. Guillemand-Mueller, et al., Proc. Int. Conf. on Nuclei Far from Stability, Lake Rosseau, Ontario, p. 757(1987); and other references therein.
3. W. Mittig, et al., Proc. 5th Int. Conf. on Nuclei Far from Stability, Lake Rosseau, Ontario, p. 11(1987).
4. H. Geissel, et al., A Proposal for a Fragment Separator for SIS-18, GSI Internal Report.
5. K.-H. Schmidt, E. Hanelt, H. Geissel, G. Muenzenberg and J.P. Defour, NIM 260,287(1987).
6. B.M. Sherrill, et al., Proc. First Int. Conf. on Radioactive Nuclear Beams, 1989, Berkeley J.M. Nitscke, Ed., World Scientific, in press.
7. K. Suemmerer and D.J. Morrissey, Proc. First Int. Conf. on Radioactive Nuclear Beams, 1989, Berkeley, J.M. Nitscke, Ed., World Scientific, in press.
8. A.S. Goldhaber and H.H. Heckmann, Annl. Rev. Nucl. Part. Sci. 28,161(1978).
9. K. vanBibber, et al., Phys. Rev. Lett. 43,840(1979).
10. D. Guillemaud-Mueller, et al., Z. Phys. 332,189(1989.
11. M. Langevin, et al., Nucl. Phys. A455,149(1986).

THE PHASE-II REACTION PRODUCT MASS SEPARATOR

R. Harkewicz, S. Bricker, D.J. Morrissey, J. Nolen, B. Sherrill and D. Swan

The Reaction Product Mass Separator (RPMS) at the NSCL is a device which physically separates heavy-ion reaction products according to their mass-to-charge ratio and focuses them to a small spot in the focal plane where detectors can be located. In last year's Annual Report we described developements in the area of RPMS beam diagnostics, detector hardware developement and we discussed improvements of the RPMS that would be attempted during the up coming NSCL PhaseII construction. In this report, we summarize the improvements that have taken place during the past year.

As part of PhaseII construction, it was necessary to disassemble the entire RPMS and move it to a new experimental floor location; we took advantage of this to reassemble a much improved device. In particular, the voltage holding capabilities of the Wien filter (velocity filter) have been greatly enhanced. This improvement was brought about mostly by replacing the glass cathode plate of the filter with a stainless steel plate. When the RPMS was disassembled it was discovered that a metallic coating on the glass plate was flaking-off and degrading performance. Now with the stainless steel plate installed we have been able to attain a much higher electric field; +145kV / -145kV across a 10 cm. plate gap, whereas +50kV / -50kV was typical before. This, of course, allows for a greater separating capability of the RPMS. Other improvements on the high voltage system included redesigning the cages on the high voltage stacks and the vacuum feedthroughs and one of the high voltage supplies was returned to the manufacturer for reconditioning.

The cooling water and vacuum system for the RPMS have been completely replumbed. A new vacuum control system has been installed that can be operated entirely by remote control from outside the RPMS vault. We have also designed and installed a new mechanical system which allows for a more accurate and trouble-free spectrometer angle movement. We are currently conducting optics tests with alpha sources with the goal of establishing a beam optics program for the RPMS. This should allow for a more efficient and accurate tuning of the device during actual experiments.

Finally, one remaining task is to complete a shielding wall between the end of the Wien filter and the final dipole magnet of the RPMS. This wall will serve to shield the focal plane detector system from any stray radiation during the separation process. We have designed and are presently beginning construction of a neutron detection array which will be located at the focal plane of the RPMS and enclose a solid angle of approximately 1.9 steradians. We will use this array to begin a systematic study of the decay of neutron-rich nuclei at the NSCL.

OPERATION OF THE PHASE 1.5 BEAMLINE MAGNETS AS A 0-DEGREE SPECTROMETER; MEASUREMENTS OF PROJECTILE FRAGMENT DISTRIBUTIONS

G.A. Souliotis, D.J. Morrissey, B.M. Sherrill and D. Mikolas

Projectile-like fragments are produced in peripheral collisions at intermediate and high energies. At high energies there is a rather complete and systematic data set of the fragmentation distributions which have been succesfully described by several models[1,2]. At intermediate energies, in contrast, there are a few scattered measurements[3] and a lack of systematic parametrization and understanding of the reaction dynamics. At these energies, the existing data indicate that transfer reaction channels compete with the classical fragmentation mechanism. In order to understand the role of the different reaction mechanisms of peripheral collisions at intermediate energies, systematic measurements are necessary. Since the projectile-like isotopes are produced in a narrow cone at 0°, refined measurements in this angular region are necessary for this study.

Towards this end before the completion of the A1200, we performed a preliminary experiment, in which the interim vault (phase 1.5) beamline magnets from the K1200 to the 92" scattering chamber were operated as a 0-degree spectrometer (Fig. 1). Projectile fragments, produced in a fragmentation target placed at the exit of the K1200, traveled through the device and were focused and detected inside the 92" chamber.

The detection system, mounted on the radial arm of the chamber, consisted of two LP-MWPC's (low pressure multiwire proportional counters) of Breskin type[4] and a ΔE-E plastic scintillator telescope. The front LP-MWPC (near the entrance of the chamber), placed at the position of the focal plane, gave momentum information. The combination of position measurements from the front and the back LP-MWPC (placed 1.8 m downstream) gave angle information. Due to low efficiency of the back position counter, the back position was also measured with the ΔE scintillator, by taking the logarithmic ratio of its left and right PMT signals. The ΔE scintillator also provided Z separation. Time-of-flight (TOF) was measured relative to the K1200 cyclotron RF cycle. Due to multiple turn extraction from the cyclotron, limited TOF resolution (4-5 ns) was obtained, which limited the particle identification for Z's higher than 6.

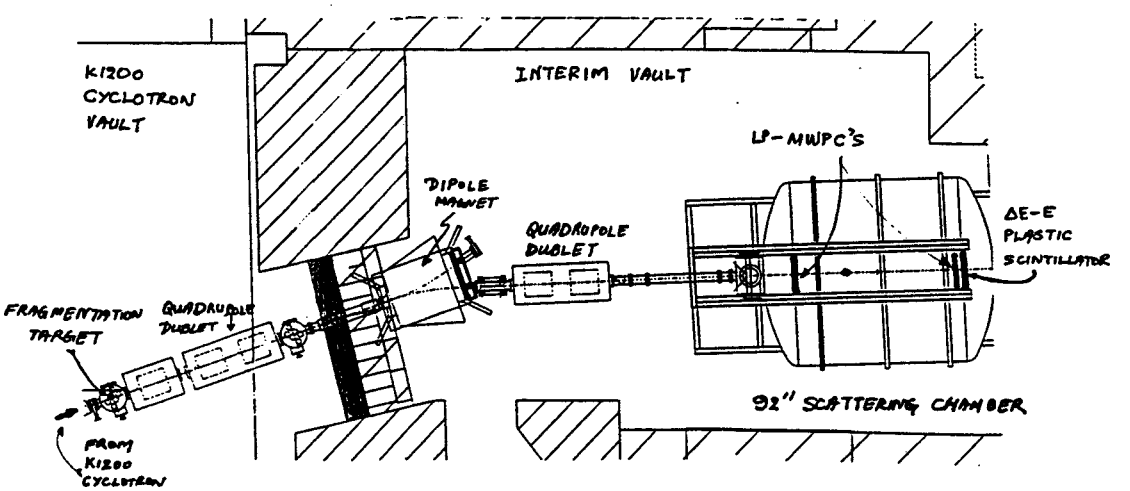

Fig. 1. Schematic layout of the interim vault (phase 1.5) beamline.

Beam optics calculations had shown that a relatively large acceptance solution was possible with this simple spectrometer, (with 35 mr and 10 mr horizontal and vertical angular acceptances, respectively, and 8% momentum acceptance). However, the presence of a non-negligible (x/θ) term, along with relatively large geometric and chromatic aberrations, made the momentum-position relation rather complicated. Unfortunately, the time restrictions under which we had to run didn't allow us to fully study the optics of the device.

In the experiment, we measured the products from ^{14}N at 75 MeV/u and ^{20}Ne at 65 MeV/u beams with Al and Ta targets. The fields of the magnets were stepped by 5% in the A/q region of 2.2-3.0. Position and angle calibrations were performed in two independent ways, giving similar results: first by rotating the radial arm (where the detector system was mounted) by a known angle and measuring the change in position of the elastic peaks, and second, by inserting a slotted copper mask (mounted on the target ladder of the chamber) and irradiating it with a dispersed primary beam.

By performing a careful off-line analysis and calculations, we were able to relate the momentum of a given particle to its position (at the first position counter) and angle. First, the position of the elastic peaks, present in several runs, gave us a rigidity-position calibration corresponding to the angle θ_b (the angle of the beam relative to the optical axis of the spectrometer). This angle was found to be 1° to the left (looking downstream the beamline). The layout of the first section of the K1200 beamline is now being corrected to bring it into alignment with the exiting beam.

In order to take into account the angle dependence of the rigidity of a particle that leaves the target, algebraic formulas were derived, which incorporated the rigidity-position calibration at angle θ_b and the angle dependences as expressed by the calculated matrix elements. As part of the above derivation, the scattering angle θ_r (relative to θ_b) of a particle was calculated. Using the derived relation for the rigidity along with the TOF (with respect to RF), an expression for A/q was also constructed.

For each isotope, a θ_r-P/q histogram was generated, θ_r cuts were made at 0°, 1° and 2°, (with width of 1° about each point) and the corresponding P/q spectra were constructed. Then, for each isotope, after normalization and proper overlay of the spectra from different runs, a P/A spectrum at each of the above angles was obtained. Finally, angular distributions were also constructed by integrating the P/A distributions at each angle.

The results of this test run show the main characteristics of the momentum and angular distributions of the projectile-like isotopes produced at intermediate energies at and near 0°. As representative results, the momentum distributions of ^{13}C, ^{15}C and ^{10}Be produced from a ^{14}N beam at 75 MeV/u on Al and Ta targets are shown in Fig. 2 and 3, respectively. We are in the process of preparing a manuscript describing the operation of the beamline as a spectrometer, including some of the results of this study.

This preliminary experiment was very informative, giving a large insight into how to operate the A1200 device, (presently under construction), indicating problems with the alignment of the beamline and the critical nature of the stability of the RF timing for the A1200. The next step in the systematic study of intermediate energy fragmentation will be to begin measurements with the A1200.

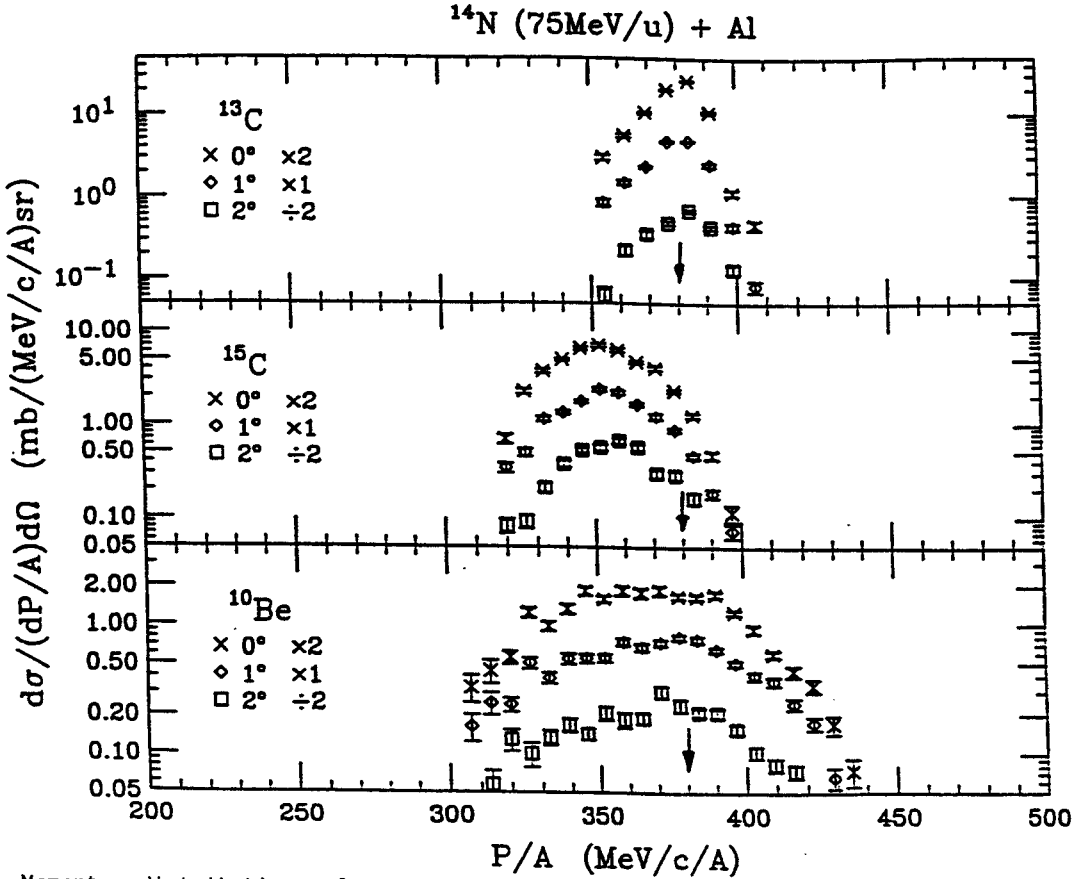

Fig. 2. Momentum distributions of some projectile-like isotopes produced from the reaction of ^{14}N at 75 MeV/u with Al target. The beam momentum is indicated by an arrow.

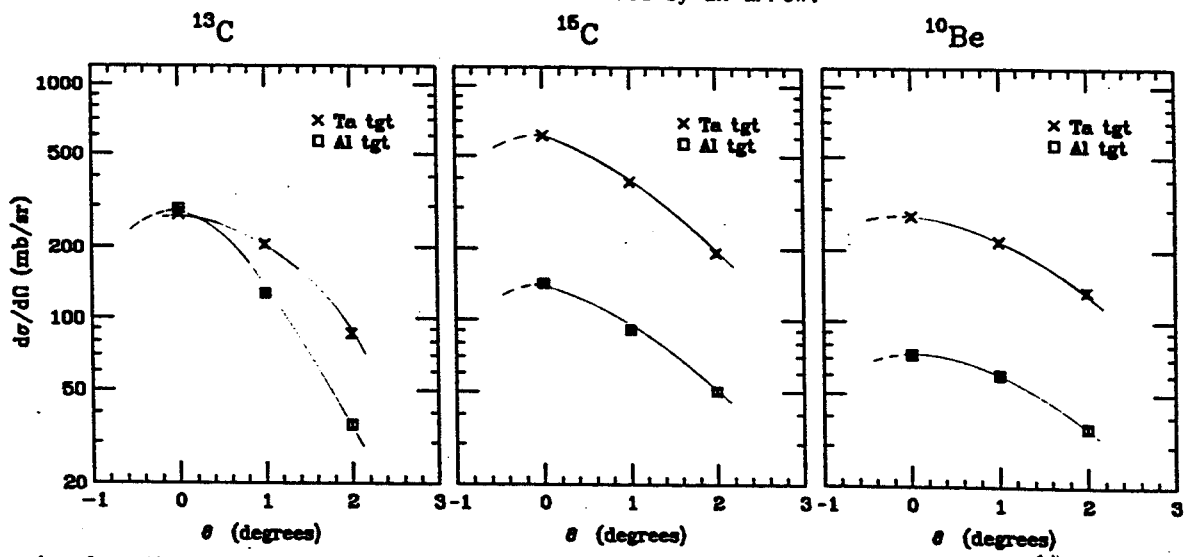

Fig. 3. Angular distributions of some projectile-like isotopes from the reaction of ^{14}N at 75 MeV/u with Al and Ta targets. At each point, the angular bin has a full-width of 1°.

References

1. J. Hufner, Phys. Rep. 125(1985)129.
2. E. Friedlander and H.H. Heckman, "Treatise on Heavy-Ion Reactions" 4, D.A. Bromley, Ed. (1987)
3. Y. Blumenfeld et al., Nucl. Phys. A455,(1986)357.
4. A.Breskin, Nucl. Instrum. Methods 196(1982)11

STATUS OF THE MSU 4π ARRAY

G.D. Westfall, S. Bricker, D.A. Cebra, J. Clayton, M. Cronqvist, D. Kataria, D. Krofcheck, R. Lacey, T. Li, M. Maier, L. Morris, T. Reposeur, D. Swan, K. Tyson, A. Vander Molen, W.K. Wilson, J. Winfield and J. Yurkon

The MSU 4π Array[1] is designed to detect as many charge particles as possible from collisions of intermediate energy heavy ions. To accomplish the task, the 4π Array contains 170 light particle detectors, 55 target-like fragment detectors, and 30 fission-fragments detectors. The light particle detectors are composed of fast/slow plastic scintillator phoswich detectors. The ΔE counters are 3 mm thick fast plastic. These counters are backed by 25 cm thick slow plastic E counters. The phoswiches are arranged in 30 separate subarrays which allows the easy substitution of other kinds of detectors by simply removing one or more of the subarrays. The target-like counters are Bragg curve counters (BCCs). The BCCs are gas ionization counters oriented such that the electric field of the counters is parallel to the trajectory of the observed particles. The BCCs use P10 gas at a pressure of 500 torr. The fission fragment counters are low pressure multi-wire proportional counters (LPMWPC) with x/y position sensitivity. Because the light particles traversing the gas counters leave very little energy, the apparatus can simultaneously detect light and heavy particles at the same angles.

To date the experiments carried out in the 4π Array have used all or most of the scintillator counters. The 170 phoswiches have been calibrated and we understand the response of the detectors very well. In addition we have been using an array of 45 phoswiches in the forward end-weldment of the Array providing a total of 215 light particle counters.

The MSU 4πm Array has been used to carry out three major experiments in the past year. The first experiment consisted of an excitation function using ^{40}Ar beams from 35 to 100 MeV/nucleon. In the second two experiments, one or more of the subarrays of the Array were removed and specialized detectors were substituted in their place. In the first of these experiments, detectors consisting of BaF_2, BGO, and Cerenkov counters were used to study the production of high energy γ-rays with event characterization. In the second specialized experiment, one of the subarrays was replaced with an array of Si detectors designed to study the production of intermediate mass fragments from central collisions.

Currently the 4π Array is being made operational in the N2 Vault after having recently operated for over a year in the Interim Vault using the K1200 Cyclotron and for a year previous to that time in another vault using the K500 Cyclotron. In the N2 Vault the 4π Array can accept beams from either cyclotron including exotic beams produced in the A1200. The MSU 4π Array is shown in Fig. 1 being installed in the N2 Vault.

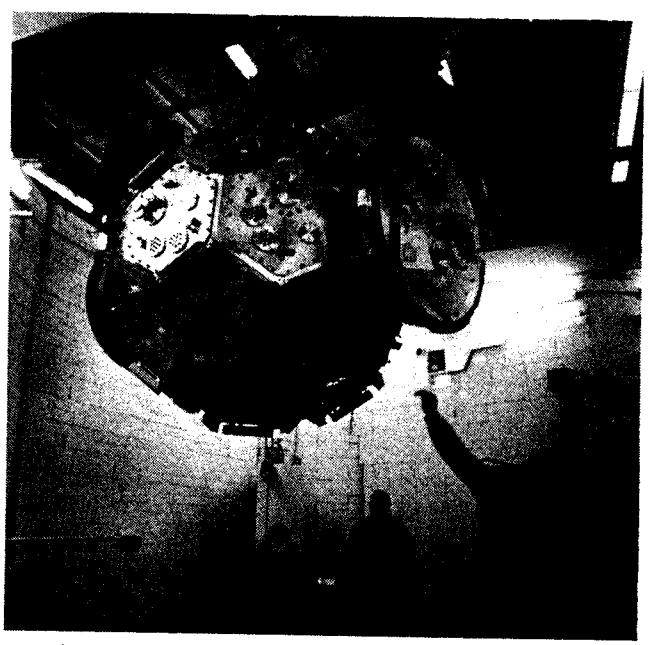

Fig. 1. Photograph of the MSU 4π Array being readied in its new location in the N2 Vault.

The BCCs are currently being installed on the front of each of the 30 subarrays. We plan to segment the anodes of the most forward five hexagonal modules giving the Array 55 separate BCCs.

A new target mechanism for the 4π Array is begin constructed that will allow the use of reactive targets such as calcium. This device will consist of a target insertion and transport arm that can service eight targets stored in a rotating carousel. These targets can be inserted into the carousel under vacuum.

We have an array of software in place that automates the startup and check out the 4π Array, as well as calibrating and setting up the ADCs and discriminators. In addition we have produced a preliminary set of documentation concerning the operation of the 4π Array.

References

1. G.D. Westfall, J.E. Yurkon, J. van der Plicht, Z.M. Koenig, B.V. Jacak, R.Fox, G.M. Crawley, M.R. Maier, B.E. Hasselquist, R.S. Tickle, and D. Horn, NIM 238(1985)347.

THE MSU MINIBALL 4π FRAGMENT DETECTION ARRAY

R.T. de Souza, N. Carlin,[a] Y.D. Kim, J. Ottarson, L. Phair, D.R. Bowman, C.K. Gelbke, W.G. Gong, W.G. Lynch, R.A. Pelak,[b] G. Poggi,[c] M.B. Tsang and H.M. Xu

In order to study multiple emission of complex fragments with nearly 4π coverage, we have constructed a fragment detection array of high granularity and low detection thresholds. In its present configuration, the device covers the angular range of θ_{lab} = 9°-160° with 188 phoswich detectors consisting of 40 μm thick plastic scintillator foils and 2 cm thick CsI(Tl) scintillators. Thresholds for particle identification range from E/A≈1.5 MeV for alpha particles to E/A≈3 MeV for Ca ions. Individual detectors can resolve elements from Z≈1-18, as well as isotopes of hydrogen and helium.

An artist's perspective of the three-dimensional geometrical assembly is shown in Fig. 1. The array consists of 11 independent rings coaxial about the beam axis. For ease of assembly, as well as servicing, the individual rings are mounted on separate base plates which slide on two precision rails. Good thermal conductivity between detectors and the mounting structure allows the conduction of heat generated by the photomultiplier voltage divider network into the array superstructure. This heat is removed from the Miniball by cooling the base plates.

Figure 2 shows a half-plane section of the array in the vertical plane which contains the beam axis. Individual rings are labelled by the ring numbers 1-11 which increase from forward to backward angles. For each ring, the number of detectors is given in parentheses. For a given ring, the detectors are identical in shape and have the same polar angle coordinates with respect to the beam axis; these angles are indicated in Fig. 2. Since the angular

MSU-90-047

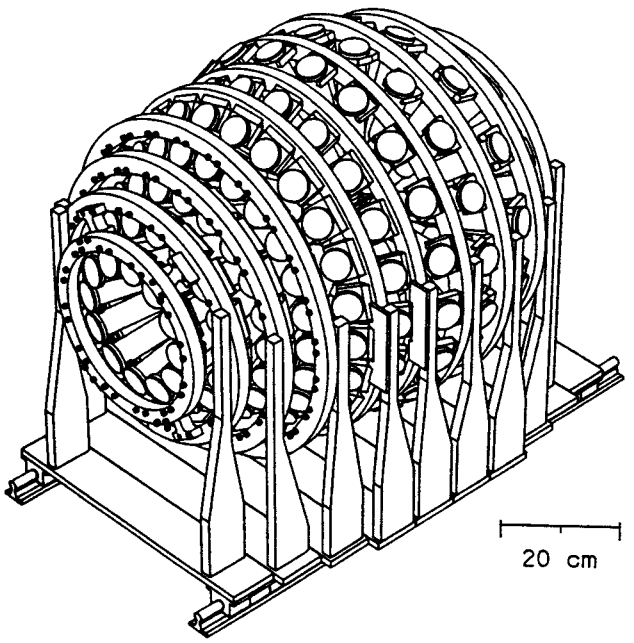

Fig. 1. Artist's perspective of the assembly structure of the Miniball 4π fragment detection array. For clarity, electrical connections, the light pulsing system, the cooling system, and the target insertion mechanism have been omitted.

MSU-90-046

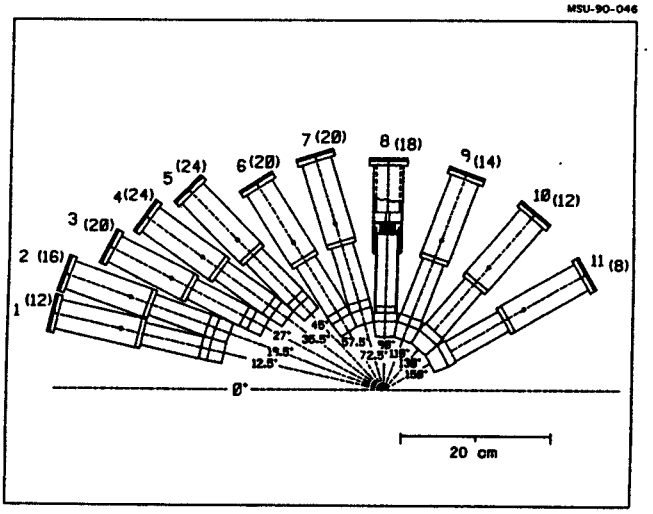

Fig. 2. Half-plane section of the Miniball array. Individual detector rings are labelled 1 through 11; numbers of detectors per ring are given in parentheses; the polar angles for the centers of the rings are indicated. The dashed horizontal line indicates the beam axis.

distributions of the emitted particles are strongly forward peaked, the solid angle subtended by forward detectors is smaller than for backward detectors. Variations in solid angle were achieved largely by placing detectors at different distances from the target while keeping their size approximately constant. In its present configuration, the detector array covers a solid angle corresponding to about 89% of 4π.

An isometric drawing of the target insertion mechanism is shown in Fig. 3. The targets are mounted on frames made of flat shim stock of 0.2 mm thickness. Each target frame is attached to an insertion rod. The insertion rods are mounted on a tray which can be moved parallel to the beam axis. An electromagnetic clutch provides the coupling to the insertion and retraction drive once a target rod is located at the appropriate position. A third drive allows rotation of an inserted target about the axis of the insertion rod.

Figure 4 shows a block diagram of the data acquisition electronics. The anode current from the photomultipliers is split via passive splitters into into the "fast", "slow", "tail", and "trigger" branches of relative amplitudes $I_{fast}:I_{slow}:I_{tail}:I_{trig} \approx 0.82:0.04:0.04:0.1$. The "slow" and "tail" branches are connected

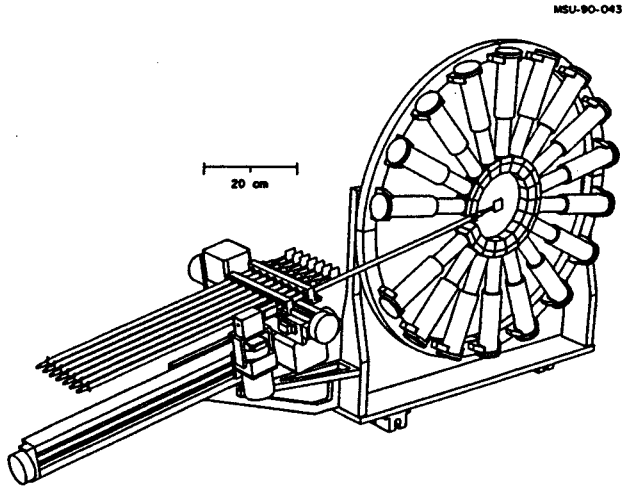

Fig. 3. Isometric view of the target insertion mechanism.

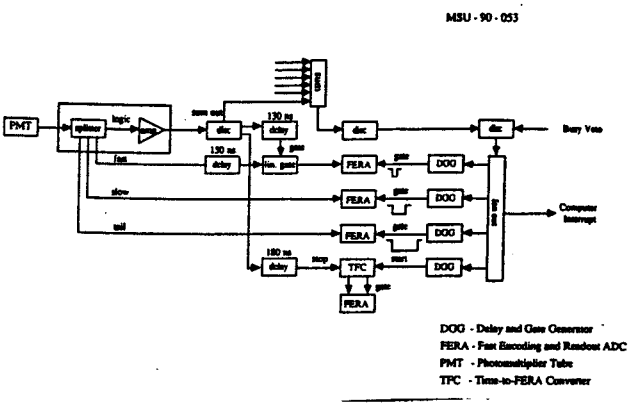

Fig. 4. Schematic diagram of the data acquisition electronics of the Miniball.

directly from the splitter to their respective fast encoding readout analog-to-digital converters (FERAs). The gates for the "slow" and "tail" FERAs are 400 ns and 2 µs wide and open 200 ns and 2 µs after the leading edge of the linear signal, respectively. For the "fast" branch, a linear gate is inserted between the passive splitter and the "fast" FERA. This linear gate allows the individual gating of each "fast" channel which cannot be achieved with the common gate FERAs. The linear gate is opened 5 ns prior to the leading edge of the linear signal and for a duration of 35 ns. The "fast" FERA is gated by a common gate of 100 ns width which begins approximately 35 ns prior to the leading edge of the linear input signal. The trigger branch, I_{trig}, is re-amplified by a fast amplifier and fed into a leading edge discriminator module, the output of which provides the stop signal for the time-to-FERA-converter and opens the linear gate for the "fast" channel.

Each discriminator module provides a sum output for its 16 channels. The amplitude of this sum signal is proportional to the number of channels which have triggered. By setting a discriminator level on the linear addition of all discriminator sum outputs, a simple multiplicity trigger is obtained.

In order to reduce dispersive losses for the fast anode current pulse representing the response of the plastic scintillator, the data acquisition electronics is located close to the measurement station. Discriminator thresholds and photomultiplier gains are adjusted via remote computer control. Remote inspection of each detector signal is possible by using the sum output of the linear gate modules and selective masking the discriminators.

The particle identification resolution of various phoswich detectors was tested for fragments emitted at about θ_{lab}=35° in the $^{40}Ar+^{197}Au$ reaction at E/A=35 MeV. All data were taken with the standard electronics setup described in the previous section. Part (a) of Fig. 5 shows a two-dimensional plot of the "fast" versus the "slow" charge integration parameters for a phoswich consisting of a 4 mg/cm^2 scintillator foil glued to the CsI(Tl) crystal. Elemental identification up to Z=18 is achieved over a considerable dynamical range of particle energies. Part (b) of the figure shows a linearized presentation of these data which is more suitable to display the resolution of the device. From such a linearized presentation, projections on the particle identification axis can be generated which show the particle identification resolution in a more quantitative form.

Spectra projected on the particle identification axis are shown in Fig. 6. Part (a) of the figure shows the projection of the data displayed in Fig. 5; part (b) show the result for a phoswich using a 4 mg/cm^2 scintillator foil without glue bond. Better resolution is obtained by using a glue bond between the scintillator foil and the CsI(Tl) crystal. Additional improvements in particle identification resolution can be achieved by increasing the thickness of the scintillator foil. For a specific experiment, the benefits of improved particle identification resolution

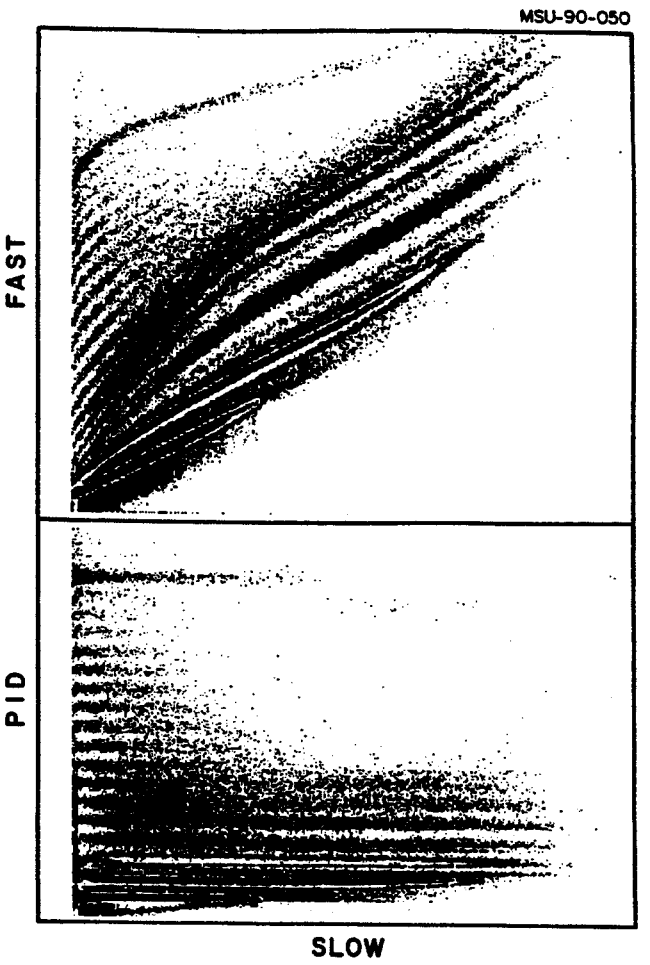

Fig. 5. Particle identification obtained from two-dimensional "fast" vs. "slow" matrix for reaction products emitted at θ_{lab}=35° for the $^{40}Ar+^{197}Au$ reaction at E/A=35 MeV; a scintillator foil of 4 mg/cm^2 areal density was used with a thin glue coupling to the CsI(Tl) crystal. (a) Matrix of raw data. (b) Linearized matrix. An intensity threshold of 2 counts per channel has been set.

due to an increase in scintillator foil thickness must be weighed against the ensuing higher energy threshold. We have also explored the use of thinner foils and found that the resolution deteriorates rapidly for scintillator foils thinner than 3 mg/cm^2. For most purposes, particle identification provided by foils of 4 mg/cm^2 thickness is satisfactory.

The use of thin scintillator foils in phoswich detectors for particle identification

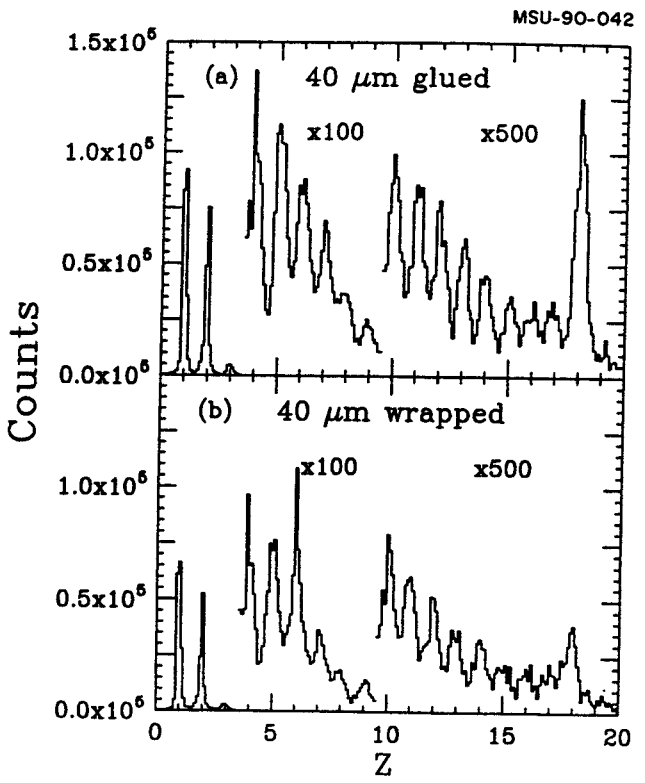

Fig. 6. Projections of linearized particle identification spectra for reaction products emitted in the $^{40}Ar+^{197}Au$ reaction at $\theta_{lab} \approx 35°$ obtained with phoswich detectors using scintillator foils of 4 mg/cm^2 thickness, (a) with and (b) without glue coupling between the scintillator foil and the CsI(Tl) crystal.

is complicated by the fact that the fast plastic scintillator signal is superimposed on the rising signal from the CsI(Tl) scintillator. Good particle identification via direct charge integration depends critically on well defined integration times. Electronic walk introduced by leading edge discriminators changes the detailed shape of a particle identification line in the "fast" versus "slow" matrix, but it has only minor effects on the separation between adjacent particle identification lines. Time jitter in the integration gate, however, does have an adverse effect on the particle identification resolution, since it produces fluctuations in the amount of CsI(Tl) scintillation integrated by the fast time gate. If the fast component is integrated by ADCs with a common gate mode, loss in resolution will occur whenever there is a time jitter between gates provided by different channels. Loss in resolution will be inevitable when more than two detected particles with different flight times are converted in separate channels of a common gate ADC. The problem can be avoided by introducing linear gates into the "fast" channel which are individually opened (see Fig. 4).

Figure 7 illustrates the sensitivity of the particle identification to time jitter in the integration gate for the "fast" channel. The solid curves correspond to the centers of selected particle identification lines in the "fast" versus "slow" matrix (see, e.g. Fig. 5). The dashed curves show how these particle identification lines are shifted when the gate of the "fast" ADC arrives two 2 ns later in time. (In these two measurements, the gate width was kept constant.) Even a 2 ns time jitter in the "fast" gate is sufficient to mix the particle identification lines of neighboring elements in the "fast" versus "slow" matrix.

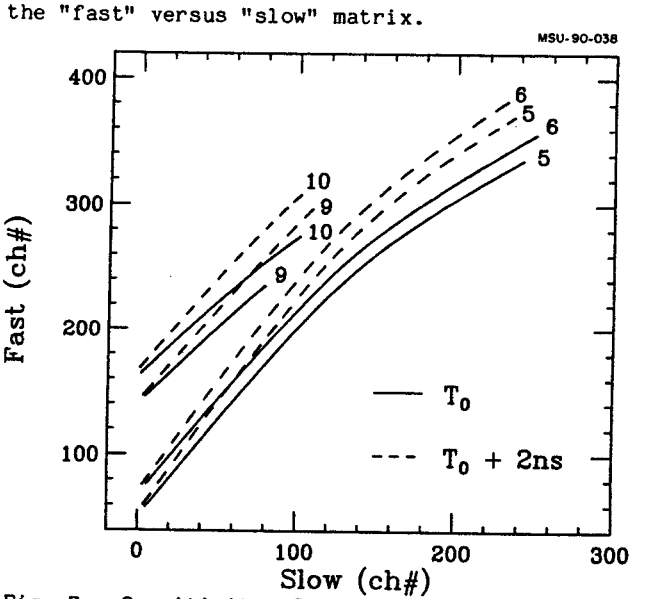

Fig. 7. Sensitivity of particle identification to time shift of the "fast" charge integration gate. The solid and dashed lines show the loci of representative particle identification lines in the "fast" vs. "slow" identification matrix obtained for gates displaced by 2 ns with respect to each other.

Identification of hydrogen and helium isotopes is obtained by standard pulse shape discrimination techniques which make use of the fact that the temporal decay of the CsI(Tl) light output depends on the ionization density of the detected particles. As an example, Fig. 8 shows the particle identification obtained from a two-dimensional matrix of the "slow" versus "tail" parameters.

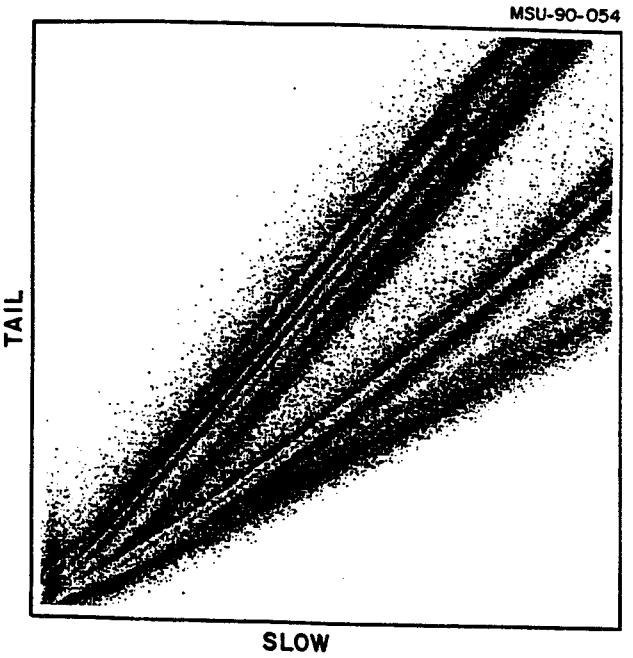

Fig. 8. Particle identification obtained from two-dimensional "slow" vs. "tail" matrix for reaction products emitted at θ_{lab}=35° for the $^{40}Ar+^{197}Au$ reaction at E/A=35 MeV.

---

a. University of São Paulo, Brazil
b. Now at: Cornell University, Ithaca, NY 14853, USA
c. University of Florence, Italy

SCINTILLATOR FOIL FABRICATION FOR THE MSU MINIBALL

Y.D. Kim, N. Carlin,[a] R.T. DeSouza, R.A. Pelak,[b]
C.K. Gelbke, W.G. Lynch and M.B. Tsang

Thin and homogenous scintillator foils for the MSU Miniball detector were spun[1,2] from Betapaint, Bicron BC-498X plastic scintillator dissolved in xylene. The original solution was ordered with a 40% weight ratio of solute to solvent. It was then diluted by adding xylene until the solution had the desired viscosity of 20-30 poise.

The viscosity was determined by measuring the terminal speed, v, of a steel ball sinking in a glass tube filled with a sample of Betapaint. Correcting Stoke's Law for the finite diameter of the glass tube gives the following expression for the viscosity[3]:

$$\eta = \frac{2gr^2(\rho_o-\rho)}{9v}\left(1-2.104\left(\frac{r}{R}\right)+2.09\left(\frac{r}{R}\right)^3-0.95\left(\frac{r}{R}\right)^5\right) .$$

Here, η denotes the viscosity, r and R are the diameters of the steel ball and the glass tube, g is the gravitational acceleration, and ρ_o and ρ are the densities of the steel ball and the Betapaint, respectively.

For the fabrication of scintillator foils, a glass plate of 23 cm diameter was mounted horizontally on a small platform connected to the drive of an electrical motor which allowed spinning of the plate about its center at a preselected speed. To facilitate the removal of spun foils the glass plate was covered successively with metasilicate solution and Teepol 610 and then wiped to leave only a thin film of the releasing agents on the glass substrate. An appropriate amount of beta paint was poured on the center of a glass plate. In order to provide rapid spreading of the initial solution, the plate was spun at an enhanced speed for the first few seconds until the entire plate was covered with Betapaint. Following this rapid startup, the glass plate was spun at the preset rotational frequency for a duration of approximately 4 min until a solid foil had formed. After spinning, the glass plate was stored in a flow of dry nitrogen for a duration of about eight hours. The foil was then peeled from the glass plate, mounted on a frame, and placed in a dry nitrogen atmosphere for another 24 hours to allow further evaporation of residual xylene.

We obtained good and reproducible results by using more dilute solutions and by spinning at lower rotational frequencies than described in Ref. 2. A number of measurements were performed to determine the relation between rotational frequency and foil thickness in this operating range. The results of these measurements are shown in Fig. 1. For each foil, thickness and homogeneity were determined by scanning the foil in vacuum with a collimated ^{228}Th α-source, and measuring the energy of the

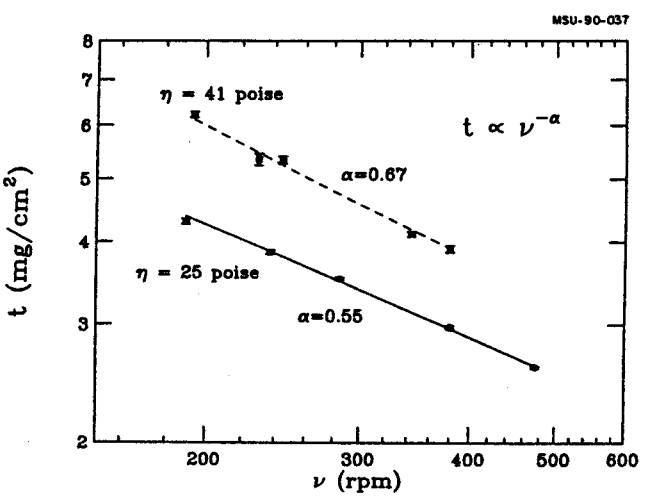

Fig. 1. Relation between scintillator foil thickness and rotational frequency of spinning measured for solutions of Betapaint of different viscosity. The lines show fits with the power law expression, $t \propto \nu^{-\alpha}$.

transmitted α-particles in a calibrated silicon detector. The energy loss in the foil was then converted to an areal density according to Ref. 4. The spun foils were uniform in thickness to within typically 1-2% over an area of 7×7 cm^2. Scintillator foils used for instrumenting the Miniball in its present configuration were selected to have a thickness of 4.0 ± 0.12 mg/cm^2.

We have explored the light collection efficiency for scintillator foils placed with and without optical cement on the front faces of the CsI(Tl) scintillators. Considerable effort was spent on developing a technique which provides an optically clear glue bond of minimum thickness between the plastic scintillator foil and CsI(Tl) crystal. Best results were obtained with Epo-tek 301 which has a low viscosity of 1 poise and a curing time of 1 day. A thin layer of the epoxy was distributed on the scintillator foil by spin coating. By means of a thin rubber pad and a weight, the epoxy coated foil was pressed onto the CsI(Tl) crystal in vacuum and cured in a clean and dry nitrogen atmosphere. The pressure applied by the weight was typically 13 kPa. Glue layers of 300-500 $\mu g/cm^2$ areal density were achieved, with nonuniformities of the order of 50%.

We investigated the position dependence of the light collection efficiency for phoswich detectors prepared with and without glue bonds between the plastic scintillator foil and the CsI(Tl) crystal, by measuring the response at various locations on the front face (labelled 1 through 11 in Fig. 2). The upper and lower panels in Fig. 2 show the relative variations of the plastic scintillator response (integrated over the time interval Δt_{fast} = 0-50 ns) and the fast CsI(Tl) component (integrated over the time interval Δt_{slow} = 60-400 ns) for α-particles sampling different locations of a phoswich fabricated with (upper panel) and without (lower panel) a glue bond between the two

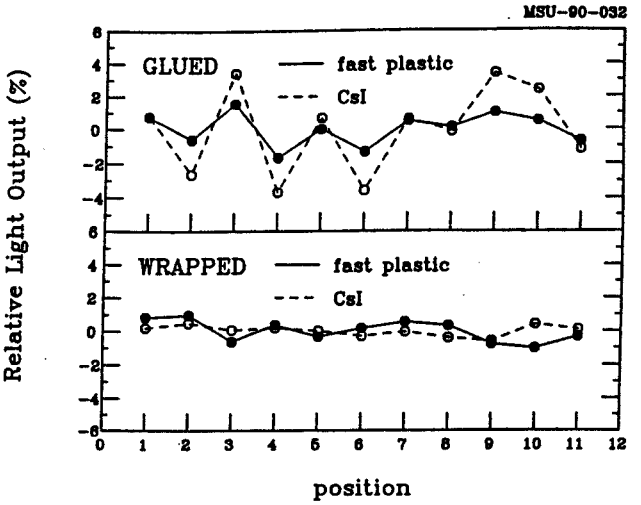

Fig. 2. Position dependent response of phoswich detectors with (upper panel) and without (lower panel) glue bond between plastic and CsI(Tl) scintillators. Solid and open points show charges integrated by the "fast" and "slow" time gates, Δt_{fast}=0-50 ns and Δt_{slow}=60-400 ns, respectively. The same foil and CsI(Tl) crystal were used in this test. Various positions sampling the entrance window are labelled 1-11.

scintillators. Both detectors have sufficient uniformity of response to provide good particle identification. In this bench test, a better uniformity of response was obtained for the phoswich without glue bond. Somewhat larger (but still tolerable) fluctuations are observed when a glue bond is applied. The observed fluctuations can be attributed to thickness variations of the glue layer which cause variations in energy deposition in the stopping CsI(Tl) scintillator (see open points in the top panel). Since some of the CsI(Tl) signal overlaps in time with the fast plastic scintillator signal, a correlated modulation appears in the charge integrated by the fast time gate. For more energetic particles, this effect should be less important as the energy loss in the glue layer decreases.

The fabrication of phoswich detectors without glue bond has the advantage of allowing changes in scintillator foil thickness to be made relatively easily. Glued phoswich detectors, on the other hand, are mechanically

more rugged. In our test runs, improved particle identification was obtained with glued phoswich detectors. However, these improvements do not appear to be compelling enough to justify the initial use of glue bonds in the Miniball array.

---

a. University of São Paulo, Brazil

b. Cornell University, Ithaca, NY 14853, USA

References

1. D. Meyerhofer, J. Appl. Phys. 49 (1978) 3993.
2. E. Norbeck, T.P. Dubbs, and L.G. Sobotka, Nucl. Instr. and Meth. A262 (1987) 564.
3. A. Dinsdale and F. Moore, Viscosity and its Measurement (Chapman-Hill, London, 1962).
4. U. Littmark and J.F. Ziegler, "Handbook of Range Distributions for Energetic Ions in All Elements", Volume 6 of "The Stopping and Ranges of Ions in Matter", edited by J.F. Ziegler, Pergamon Press, New York, 1980.

LIGHT PULSING SYSTEM FOR THE MSU MINIBALL

L. Phair, T. Peterson,[a] R.T. de Souza, N. Carlin,[b] Y.D. Kim,
C.K. Gelbke and W.G. Lynch

Gain drifts of the photomultiplier tubes in the MSU Miniball array are monitored by a simple and compact light pulser system which operates in vacuum. In order to preserve the modularity of the device and avoid unnecessary removal of optical fibers during transport, each detector ring is provided with its own light pulser system. Figure 1 shows schematics of the mechanical assembly of the light pulser system and of the driving circuit for the light emitting diodes (LEDs) which is triggered by an external NIM logic signal. During experiments, the light pulser is triggered at a rate of about 1 Hz. Light is generated by simultaneously pulsing an array of eight LEDs (Hewlett Packard HLMP-3950) which generate light at wavelengths around 565 nm. The emitted light is diffused by reflection from an inclined teflon surface. Light fibers which only view scattered light transport the light to the individual photomultipliers.

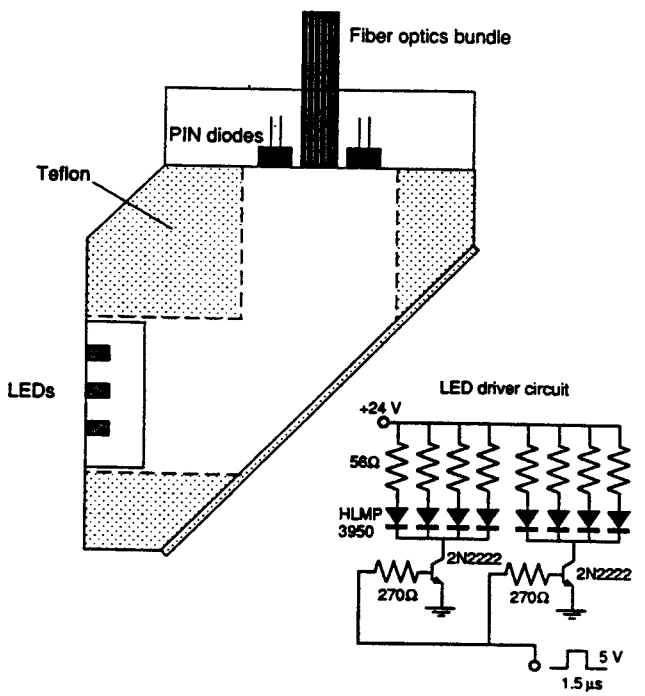

Fig. 1. Schematics of light pulser assembly and LED trigger circuit.

Because of temperature fluctuations and aging effects, operation of light emitting diodes is not stable over long periods of time. Therefore, the intensity of each light pulse is monitored by two PIN diodes (Hamamatsu S1223) read out by standard solid state detector electronics. The ratio of the signals of the two PIN diodes can be used to monitor their stability. The ratio of pin diode and photomultiplier signals can then be used to monitor the gain of the individual photomultiplier tubes according to the relation:

$$Ch' = Ch \times (Pin1+Pin2)/2Pmt \ .$$

Here, Ch denotes the ADC conversion measured for a given event, Ch' is the conversion corrected for gain shifts, and Pmt, Pin1, and Pin2, are the channel numbers for LED generated light pulses detected by the individual photomultiplier tube and the two PIN diodes, respectively. Better than 1% gain stabilization is achieved if the temperature of the CsI(Tl) crystals is kept constant. (Variations of the scintillation efficiency of CsI(Tl) caused by temperature fluctuations cannot be detected with the light pulser.) It was verified, however, that active cooling of the base plate ensures rapid achievement of a stable operating temperature for the Miniball.

Figure 2 illustrates the gain stabilization achieved with the light pulser system. The gain variations of a photomultiplier (enhanced by variations of the supply voltage) were directly measured by irradiating a CsI(Tl) crystal with α-particles emitted from a collimated ^{228}Th source and monitoring the peak location of the

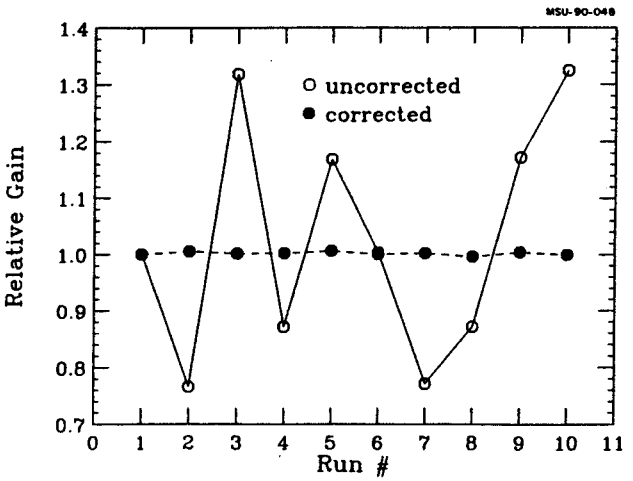

Fig. 2. Open points: gain variations of a CsI(Tl) photomultiplier assembly determined by measuring the detector response to 8.785 MeV α-particles; solid points: same data corrected for gain shifts in the off-line analysis by using information from the light pulser system.

8.785 MeV α-line; they are shown by the open points in the figure. The solid points in the figure show the peak positions obtained in the off-line analysis after correcting the gain variations according to information from obtained by the light pulser system. Gain stability to better than 1% was achieved.

---

a. Gustafus Adolfus College, Saint Peter, MN 56082, USA
b. University of São Paulo, Brazil

THE S800 SPECTROGRAPH

A.F. Zeller, J.A. Nolen and B. Sherrill

The original Phase II construction grant included money for a spectrograph, the S800. Some major components such as the dipole steel were purchased. However, during Phase II construction it was decided to postpone completion of the S800 in order to add a beam analysis device and an ECR ion source to the project. Recently, a proposal has been submitted to the NSF for funds to complete the S800 spectrograph. The parameters of the spectrograph and the details of its design have been presented previously[1].

A good measure of the interest in the physics which can be studied with the S800 was the strong participation in the International Symposium on Heavy Ion Research with Magnetic Spectrographs, which was sponsored by the NSCL and held in January, 1989. There were over 100 participants from 12 countries, spanning 5 continents. The proceedings of this conference have been published as an NSCL Report No. 685. Given this interest, it is clear that a high quality, high resolution magnetic spectrograph would play a key role at the NSCL, and in the U.S. heavy ion research program.

The NSCL facility will have unique capabilities for heavy-ion studies. With the K1200 and K500 cyclotrons, experiments with beams from protons to Uranium and energies of 2 to 200 MeV/u are possible. In addition, the A1200 beam analysis device, presently under construction, will be able to measure and define precisely the beam energy, and produce separated radioactive beams which can be transported to any experimental device, including the S800.

For comparison of the S800 to other spectrographs, a figure of merit versus year of construction for various magnetic spectrographs is shown in Fig. 1. The S800, labeled MSU, is

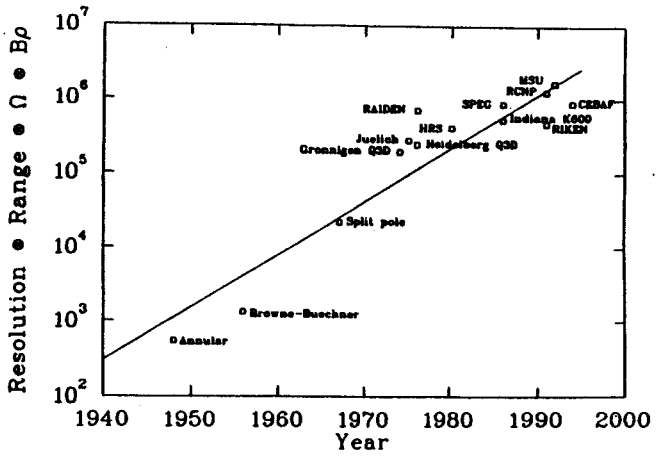

Fig. 1 Figure of merit versus year of construction for forty years of spectrograph development. The figure of merit is the product of the solid angle in msr, the resolution (assuming a 1mm object size), the energy range in percent, and the magnetic rigidity in T-m.

among the best in terms of its combination of solid angle, energy range, energy resolution, and magnetic rigidity.

It achieves these values, in part, because it will be the first superconducting high resolution magnetic spectrograph for nuclear physics. The spectrograph has an $E/\Delta E$ of 10^4 for the entire 20 msr solid angle. This has been demonstrated by raytracing and by a simulation of software corrections through the use of the optimization computer code MOTER.

The S800 has a QQDD configuration with the quadrupoles labelled Q1 and Q2 or QY and QX in the following discussions and figures. The quadrupoles require large gradients and/or large apertures. This necessitates the use of superconducting magnets, since space is not available for longer quads. The first step in considering the iron dominated quad option is to simply scale-up beamline quads to have the

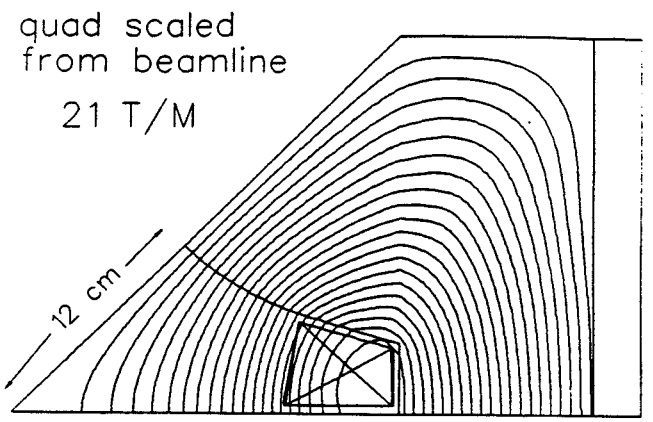

Fig. 2 The NSCL beamline quad scaled up in size for Q1.

necessary diameter for use as Q1. A POISSON calculation or this is shown in Fig. 2. Note that the field lines are not parallel to the front edge of the coil, while in the beamline quads they are. This is a consequence of having the iron pole tip at a field of 2.5 T. We know that dipole magnets can always be optimized for a given field level, even in the non-linear region of 1.7 - 3 T. However, to have a large dynamic range magnet two or more coils must be used, as in the Texas Accelerator Center's "Superferric" SSC dipole[2]. The same thing is true for the beamline quadrupoles. Figure 3 shows a modified beamline quad which has two coils, which run with the same polarity. At different gradients the ratio of currents is different to account for saturation. Shown in Fig. 4 is a comparison of the two types. The Q17 is the two coil design and the BL is the beamline design. It must be stressed that the Q17 design is not fully optimized, since a higher current density design could achieve better uniformity. Modification of the coil sizes, positions, and the notch size are on going and are expected to decrease the deviations by a factor of 2-3. Further improvement in the one-coil design may be possible by considering various steel profiles and coil shape changes.

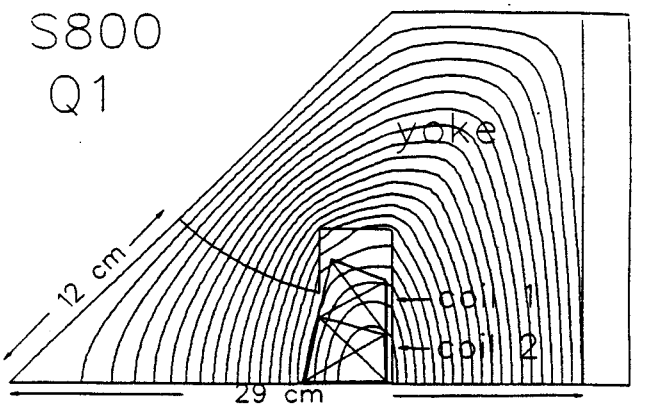

Fig. 3 A modified scaled-up beamline quad for Q1. The quad has two coils with the same polarity and a notch cut in the pole to allow for a bigger coil (to reduce current density).

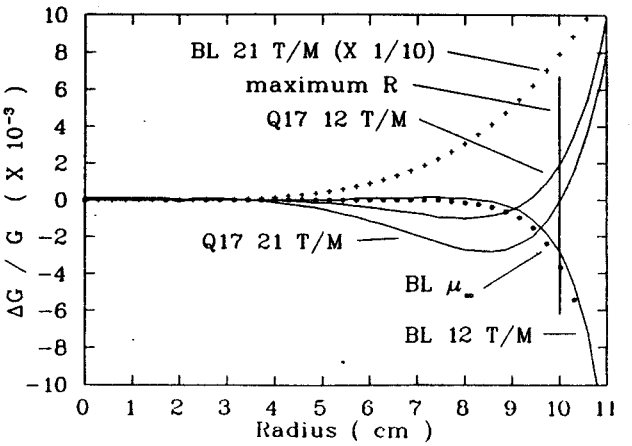

Fig. 4 A comparison of the gradient uniformities for the two types of beamline type quads. The curves labeled Q17 are for a two coil quad, and the curve with BL are quads as in Fig. 2.

In terms of simplicity, making the S800 quads scaled up versions of the successful beam line quads is preferred, if raytracing calculations indicate that the achievable field qualities are tolerable. As seen, the single coil option is significantly worse in error terms than the two coil beam line model. The single coil can be optimized somewhat by making the coil smaller and further from the median plane. This makes the low gradients more inhomogeneous and the high gradients better. The worst case error can then be used in

raytrace calculations to determine the effect on the resolutions.

A larger version of the beam line quad for Q2 implies that the radius is much larger in one dimension than necessary, but the pole tip fields are similar to the beam line quads. Thus the design is simplified and the low current density allows the quad to operate safely at higher gradients if needed, e.g. for an intermediate detector option and to compensate for three dimensional effects. Three dimensional field calculations of these quadrupoles, probably with the code TOSCA, will be done before these designs are finalized.

In order to study the uncorrected system more carefully and, in particular, to see what happens when rays are traced through to a focal plane which has two detectors with finite resolution, the optimizing code MOTER[3] was used. This code allows the input of 400 rays with a set of random measurement errors for each ray. This is equivalent to using up to 3600 rays. For our simulations, various focal plane measurement uncertainties (FWHM) were assumed: Δx = 0.2 to 0.4 mm, Δy = 0.4 mm and $\Delta\theta = \Delta\phi$ = 0.3 to 1 mr. Note that Δx primarily causes momentum measurement error and Δy primarily angular measurement error. The quantities $\Delta\theta$ and $\Delta\phi$ are the measurement precision of angles at the focal plane. One then "corrects" for dispersion matching, focal plane tilt, and a large number of aberrations. The momentum and angular measurements are then an "error" function which consists of what is left after removing all known aberrations (to within the limits of the directors). In our study about 25 different aberrations were included for each plane.

A typical error histogram is shown in Fig. 5. For ease in comparison, a Gaussian has been fitted to the data in such a way as to preserve the standard deviation and the peak area. For each combination of solid angle and momentum

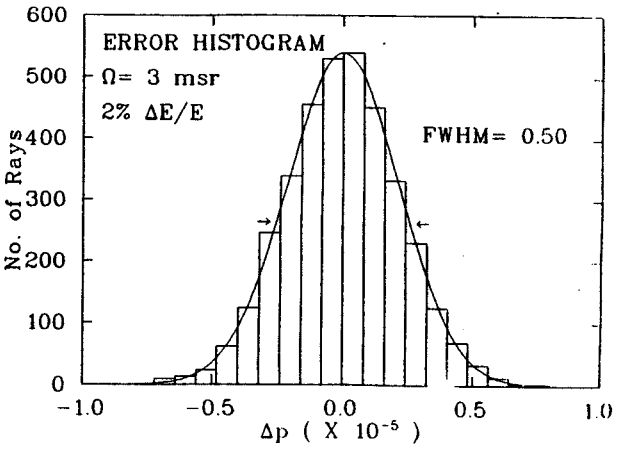

Fig. 5 Sample error histogram for momentum with a Gaussian fit to the data.

band pass, histograms are obtained for momentum resolution ($\Delta P/P$) and scattering angle resolution ($\Delta\theta$). In addition to the basic assumption of focal plane detector resolution of Δx = 0.2 mm, Δy = 0.4 mm, and $\Delta\theta = \Delta\phi$ = 1 mr(FWHM), calculations for other combinations of $\Delta x = \Delta y$ = 0.4 mm and $\Delta\theta = \Delta\phi$ = 0.6 mr (detector separation = 1m) and for $\Delta\theta = \Delta\phi$ = 0.3 mr (separation = 2 m) were done. Error functions for a typical case, 20 msr and $\delta = \pm 0.1\%$, for the three focal plane resolution assumptions are shown in Figs. 6 and 7, for the momentum and scattering angle resolution, respectively. The curves are labeled with the appropriate detector resolutions. (241 => .2 mm x, .44 mm y, and 1 mr in $\Delta\theta$ and $\Delta\phi$, etc.)

In order to test our assumptions on the strength of the allowed dipole field gradients, the calculated error gradient was included in all the calculations. Calculations are summarized in Table I for the three different detector assumptions, as well as the cases for no measurement errors ($\Delta x = \Delta y = \Delta\phi = \Delta\theta$ = 0). Also shown are some calculations for the case of no dipole errors. It should be noted that the numbers have about a 10% variation depending on the random rays chosen by the program and by the weighting factors used in the choice of optimization for momentum or scattering angle.

Table I

Raytracing Calculations of S800 Resolution

1 G/cm gradient in dipoles

	Detector Requirements				$\Delta P/P$ ($X10^{-4}$)		$\Delta\theta$ (mr)	
Ω(msr)	$\delta(\pm\%)$	x(mm)	y(mm)	$\theta=\phi$(mr)	FWTenthM	FWHM	FWTenthM	FWHM
3.6	.5	0	0	0	.32	.18	.12	.066
3.6	.5	.4	.4	.6	.91	.50	.95	.52
20	.01	.4	.4	.6	.85	.47	1.16	.64
20	.8	.2	.4	1.	.82	.45	1.70	.90
20	2.5	.4	.4	.3	1.06	.58	.97	.53
20	.1	0	0	0	.41	.22	.13	.072
20	.1	.2	.4	1.	.82	.45	1.61	.88
20	.1	.4	.4	.6	1.09	.60	1.18	.64
20	.1	.4	.4	.3	.90	.49	.93	.51
10	2.5	0	0	0	.30	.16	.12	.072
10	2.5	.2	.4	1.	.86	.47	1.15	.63
10	2.5	.4	.4	.6	1.00	.55	1.00	.55
10	2.5	.4	.4	.3	.90	.49	.93	.51
				No dipole errors				
10	2.5	0	0	0	.23	.13	.083	.046
10	2.5	.2	.4	1.	.56	.31	1.17	.64
10	2.5	.4	.4	.3	.84	.46	.96	.52

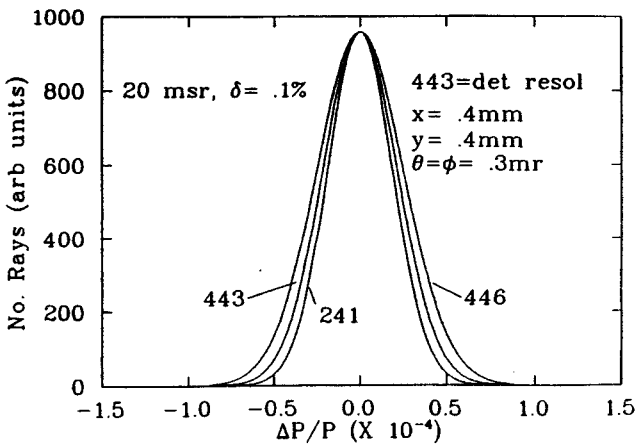

Fig. 6 Error histogram for momentum for three different detector resolution combinations.

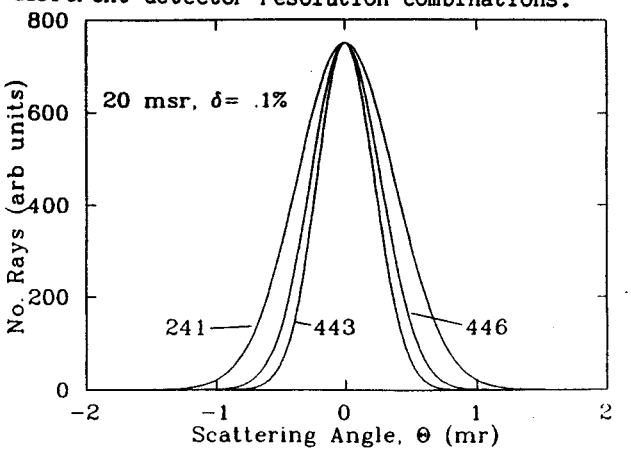

Fig. 7 Error histogram for scattering angle.

Calculations given in Table I represent several combinations which represent the normal combinations of solid angle-momentum band pass.

Additional calculations were done using the calculated field errors in the quadrupoles, using errors from the single coil scaled beamline quads, optimized with a higher current density. The worst case errors did not change the calculated resolutions by more than 3%. This is in agreement with empirical observations at HRS[4]. It can be seen from Table I that the required design goals of $\Delta E/E = 10^{-4}$ and scattering angular resolution of 1 mr are met for modest detector requirements.

For experiments which require a broader momentum acceptance the S800 design allows use of a detector between the two dipoles. This will give a broader range but lower resolution. In this mode the first order optics are point to point in both x and y planes. Using parallel to point for y leads to undesirably large detectors due to second order effects x/ϕ^2 and $y/\phi\delta$). The limiting momentum in this mode is set by the strength of the quadrupoles and gives a maximum rigidity of 0.72 GeV/c. This is equal to 67 MeV/nucleon for q/A = 1/2. Using the same detector as needed in the standard mode (50 x 15 cm^2) the band pass is $\delta = \pm 6.3\%$ corresponding to an energy range of 25%. For a ^{40}Ca beam at 67 MeV/A = 2.68 GeV this gives an excitation energy range of about 700 MeV.

With a D/M of 2.5, instead of 12 for the standard mode, the resolution is decreased to 4,200 or $\Delta E/E = 4.8 \times 10^{-4}$, assuming the same detector resolutions and configurations. The results are summarized in Table II. Note that these results have been calculated only to second order, but the small second order terms in x suggest that higher order terms are not very important. In the final quadrupole design we will give some emphasis to having higher gradients in order to extend the useful upper momentum limit of the broad range mode.

Much of the research suited to the S800 will utilize coincidence detectors around the target. Examples which illustrate the compatibility of the S800 with typical arrays of detectors are shown in Fig. 8.

To meet a wide variety of physics goals the scattering chamber geometry must be extremely flexible. The primary objective initially will be to keep the vicinity of the target as free as possible of mechanical obstructions due to support structures and bearings.

Additionally, when the spectrograph is at 0°, space for larger detectors can be gained by moving the target position further upstream from the first quadrupole. Going from the present drift length of 60 cm to 100 cm provides

Table II

Properties of spectrometer in broad range mode*

Mode:	Point-to-point in x and y
Max central momentum	0.72 GeV/c (limited by Q2)
M_x	-1.2
M_y	-10.4
D	2.96 cm/%
D/M	2.5
Focal plane tilt	30°
Δp/p (range)	±6.3%
ΔE/E (range)	±12.6%

*Assumes a 50 x 15 cm^2 focal plane and that θ_o = ±60 mr and ϕ_o = ±90 mr.

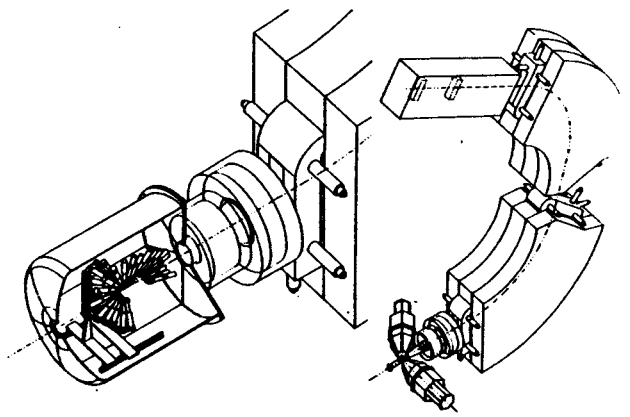

Fig. 8 Two BaF modules shown in position around the S800 target chamber. The insert shows the MSU miniball in position around the S800 target chamber and the associated cryostat for Q1.

considerably more room at a cost in solid angle. The maximum sold angle then becomes 8 msr with a momentum range reduced from 5% to 3%. Other combinations of solid angle-band pass are possible, as well as an asymmetric acceptance mode.

At the beam energies available from the K1200, most reaction products will be strongly focussed in the forward direction, thus much of the physics will be near 0°. To accommodate operation at or near 0° special Faraday cups/beam blockers are needed. There are four likely locations: 1) At a distance of about 50 cm behind the target, 2) between Q_x and D1, 3) between D1 and D2 and 4) near the focal plane. The last three of these options are shown in Fig. 9.

A Faraday cup 50 cm behind the target and 2 cm in diameter could be used for most routine angular distributions. Near 0°, however, it is better to intercept the beam between QX and D1, since a larger cup intercepting less solid angle can be used. The overall aperture of QY is 10° by 7°, so the loss of ±1/2° is not significant, unless the first 8 mr from 0° is important.

A Faraday cup can be placed between D1 and D2 if the central momentum of the product of interest differs from the beam momentum by 9% or more. For many transfer reactions this will be the case. In this case the full solid angle including 0° is available.

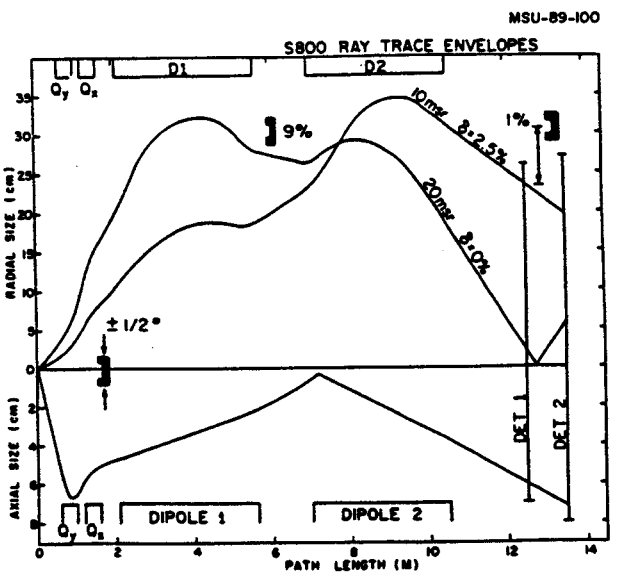

Fig. 9 Three possible locations for Faraday cups to be used in zero degree operation. One blocks ±1/2° of the aperture (10° by 7° overall) between QX and D1. The second is between D1 and D2 if the beam momentum differs from the central momentum by more than 9%. The third is near the focal plane if the momentum difference is about 1%.

A Faraday cup/shadow shield can be placed beyond the focal plane if the momentum difference is greater than about 1% as indicated in Fig. 9. Beam and/or elastic scattering peaks can be stopped immediately in front of the first focal plane detector in special cases.

References

1. A.F. Zeller and J.A. Nolen, ibid, 1981-82, 90, and references within.
2. F.R. Huson, et al., IEEE Trans. on Nucl. Sci. NS-32,3462(1985).
3. H.A. Thiessen, M. Klein and K. Boyer, LASL Report (1979) unpublished.
4. C.L. Morris and H.A. Thiessen, Los Alamos, private communication.

A LOW COST PIN PHOTODIODE/CsI(Tl) DETECTOR

J. Yurkon, G. Westfall, M. Maier, A. Mueller[a], B. Sherrill,
D. Reinhard[b] and D. Swan

The most commonly used detector for particle identification is probably an E-ΔE stack. This is often realized by a silicon detector and a scintillation detector when the particles have ranges that are too large for a stopping silicon surface barrier detector. NaI(Tl) and CsI(Tl) are commonly used scintillators due to their good uniformity and they are easily coupled to Photomultipliers. The surface barrier detector used for ΔE information, must possess good planarity, and the scintillator should have good gain stability. Gain stability for scintillators backed by photomultipliers has been difficult to obtain. They typically require gain stabilization techniques. Recently there has been a move towards using CsI(Tl) with photodiode (PD) readouts since PD's are intrinsically stable. This prompted one of us, (GW), to suggest eliminating the last photodiode and turning the device around so that the particle enter through the PD and stop in the scintillator.

Photodiodes make good planar detectors[1] and they are available in thicknesses between 300 and 1,000 microns. They can have active areas up to 25 cm^2. We have used a 1 cm^2 500 micron PD from Siemens[2] coupled to a 0.9 x 0.9 x 2.0 cm CsI(Tl) crystal as shown in Figures 1 and 2. The scintillator was wrapped with Teflon tape and placed into a Teflon case with the bare PD mounted close to the exit face. The exit was polished, and the other faces were sanded. The PD was mounted to a PC board and connections made using thermo-compression bonding with gold wires.

A test run with 40 MeV/A Ar was made in the 92" chamber. The detector was placed 20 inches from the target. The electronic setup is shown

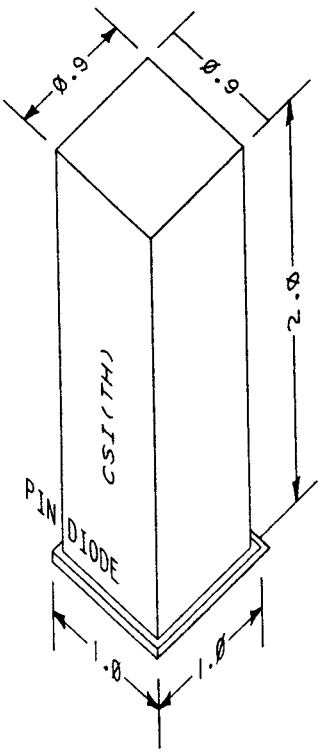

Fig. 1. The CsI PD sandwich.

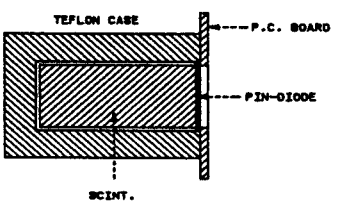

Fig. 2. Cross Section of the Complete Detector.

in Figure 3. The E and ΔE signals are separated electronically. The PD has a fast collection time compared to the slow decay component of the CsI(Tl), which is about 1,000 nanosecs. The spectroscopy amplifier was used to integrate the entire signal so it gave us the sum of the PD and the light from the scintillator. The spec. amp. section of the TC-241 was set for 3μ secs. The timing filter amplifier in the TC-241S had an integration time constant of 20 nsecs, and a

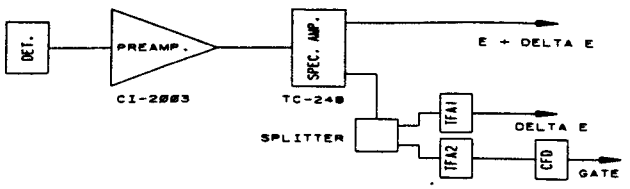

Fig. 3. Electronic Setup.

differentiation time constant of 180 nsecs to filter out the slow component to give us the ΔE signal from the PD. The TFA1 had an integration time of 100 nsecs, with no differentiation, to give a signal shape acceptable to an Ortec AD811. Because signals due to the direct interaction in the PD and the light from the scintillator have different calibrations, it was necessary to correct the display in software. (This problem can also be solved by a passive filter designed by Michael Maier.)

Figure 4 is a plot of E versus ΔE for 40 MeV/n Ar on a 30 mg Carbon target at 2 degrees. There is clear separation for all Z's. The kink in the curve is due to the gain of the TFA being set too high and beginning to saturate. This was not corrected due to the limited time we had for testing, and would not normally occur with proper gain settings. The PD had a leakage current of 70 na and after 3 hours of running with rate of 5 kcps the leakage current was 73 na.

This detector will lower the cost of high spatial resolution detector arrays and will surely be very useful in forward detector arrays.

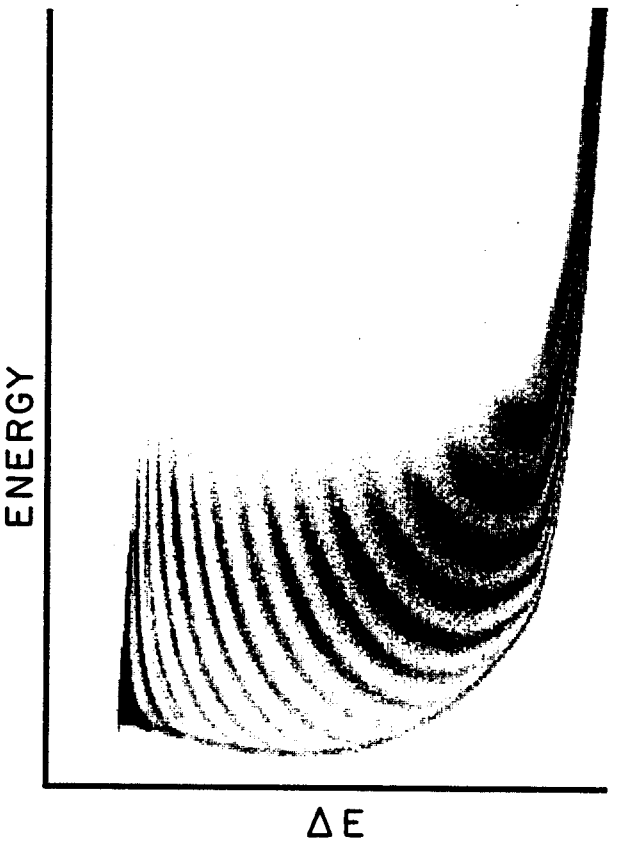

Fig. 4. E versus ΔE Histogram.

a. IPN Orsay
b. MSU Dept. of Electrical Engineering

References

1. J. Kemmer, Nucl. Inst. Meth., 169(1980)499.
2. SFH946/F109D, Siemens

LOW ENERGY π^-/π^+ 0° SPECTROGRAPH

Y. Chen, E. Kashy, W. Benenson, D. Mikolas and J. Yurkon

Pion production in intermediate energy heavy ion collisions has gernerated active research both theoretically and experimentally for the past decade. In one of the earliest experiments (Benenson et al.[1]), an anomaly in the π^-/π^+ ratio at 0° for pions of velocity near the beam velocity was found. Since that time, a significant amount of data has been obtained, and the phenomena has been observed at both higher and lower energies[2,3,4]. However it has become increasingly difficult to extend the experiment down to a beam energy of few tens of MeV per neucleon. Experiment 88017 was proposed to do just that. We report here some results of this attempt.

The experiment was carried out last November with three days of beam time. The beam was ^{40}Ar with E/A=65 MeV. The targets were 60 mg/cm^2 C and Ti. However, due to a combination of high background, low count rate and detector problems, pion events could not be identified.

The equipment used in the experiment consisted of a spectrograph and a focal plane detector system. the spectrograph separates the pions produced at 0° from heavier particles of the same energy by means of a nearly 180° deflection of the pions by the magnetic field. At the same time, it disperses the pions according to their momentum. The scheme is illustrated in Fig. 1.

The spectrograph was converted from an unused "C" shaped magnet[5]. The detector system consisted of two groups of detectors each with two multiwire detectors and a fast-slow scintillator(Phoswich). The pair of atomspheric pressure multiwire counters were placed near the focal plane so that they could measure the position and angle of particles which passed through them. Each had 0.5 cm position

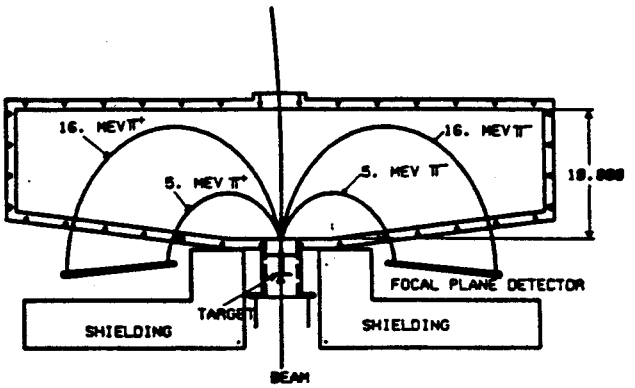

Fig. 1. Shematic drawing of the spectrograph.

resolution, and we expected that each would also give some energy loss information. The Phoswich detectors which followed the two wire counters in each group were made of a 1. mm thick fast-plastic and a wedge shaped slow plastic so that the pions from 5 MeV to 16 MeV would be stopped. The phoswich was to provide particle identification based on the energy loss in different part of the detector. The subsequent decay of pions stopped in the phoswich would further confirm our indentification. Time of flight was also used to separate real events from the background.

During the three days of the experiment, we found that, not only did the wire counters not give any meaningful energy loss information, but also the background was too high to allow any positive identification of pions. The estimated count rate of pions in the whole kinematic range of the spectrograph was about 120 per hour assuming the charged pions were produced at the same rate as π^0. At the same time, there were about 50,000 background events per hour distributed between the electron and proton PID (Particle Identification Signal) window. In this case, the straggling of electrons alone would make it impossible to identify a few pion events whose PID should be between that of an

electron and a proton. We also looked for pion decay events that would appear as very large prompt pulses from the Phoswitch on the π^- side and delayed ones on the π^+ side. Nothing was found that could be identified with such a gate.

In order to reduce the background, we tried different shielding configurations, and found that the electron background was almost isotropic, the proton events had a source near the beam exit of the chamber which suggested that some scattered particles were hitting the chamber wall. We ended the experiment after three days of running, not having succeeded in reducing the backgound further.

Based on data we had obtained, we concluded that in order to identify the few pions produced in the level of background we encountered, more independent PID's were needed. A plastic scintillator, proportional chambers and a silicon photodiode were tested with cosmic ray muons for that purpose. In all three cases, we could not achieve resolution better than 30 %. For the plastic scintillator, the fact that the thickness of the detector is limited by the range of low energy pions places a limit on the resolution we could achieve. In Fig. 2, a muon energy loss spectra from a 1 mm thick plastic scintillator is shown. Since the actual energy loss spread due to straggling is close to 30%, the observed resolution of 100% is determined by the number of photo electrons, and is consistent with a Monte Carlo calculation. Similar statistical arguments apply to the gas counters several cm thick which give similar resolutions as the scintillator. For the photodiode, the straggling of the muons sets the limit for the resolution. In Fig. 3., the muon energy loss spectra from a 300 μm thick silicon photodiode is shown. The resolution is about 30%, and the characteristic long tail towards the high energy end of straggling is also present which is the main problem if we have a lot of electron background. In conclusion, the resolution is not

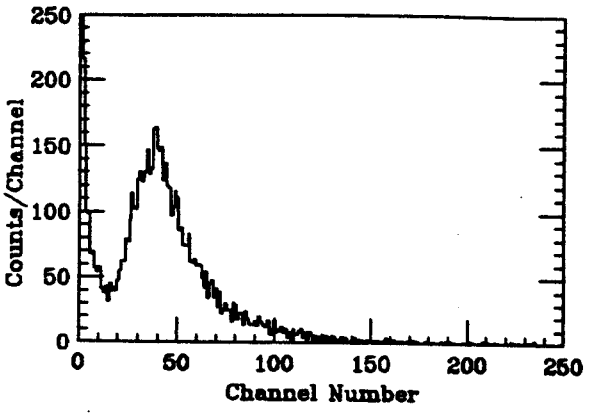

Fig. 2. Muon energy loss spectra from 1 mm thick plastic scintillator.

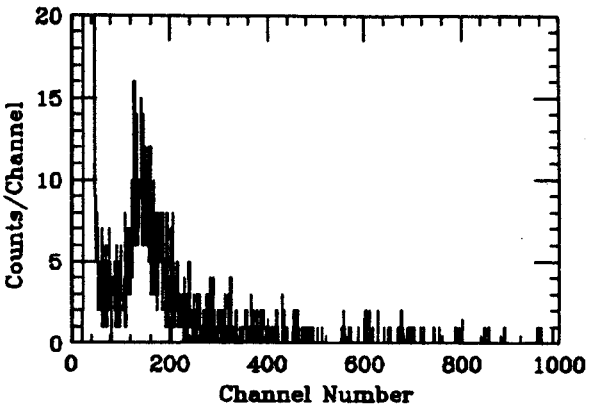

Fig. 3. Muon energy loss spectra from 3 μm thick photodiode.

sufficient to identify pions from the kind of background we expect according to our simulation. Therefore, this experiment can not be carried out successfully until significant changes in the apparatus is made.

References

1. W. Benenson et al, Phy. Rev. Lett. 43(1979)683, Phy. Rev Lett. 44(1980)543.
2. K.A. Frankel et al, Phy. Rev C32(1985)975.
3. E. Chiavassa et al, Nucl. Phys. A422(1984)621
4. S. Nagamiya et al, Phy. Rev. C24(1981)931.
5. Y. Chen et al, NSCL Annu. Rep. (1987).

NUCLEAR ELECTRONICS

M.R. Maier, D.J. Morrissey, K. Niemeyer[a], M. Robertson and James Vincent

The last year has been an especially productive one for the Research Electronics Group. During this period the group completed several major design and fabrication jobs in addition to numerous small support tasks. As an indication of the utility of the modules that we are developing, some modules have been "sold" to groups at other laboratories. We are also developing prototype modules for the APEX electron/positron experiment at Argonne National Lab.

Notable projects that were recently completed are the 25 units of the quad-shaper fast/slow amplifiers (Version 2), the fast decision module and the FERA Faucet-Maier. The quad-shapers incorporate four independent channels of timing filter plus slow shaping amplifiers into a single-width NIM package; 5 of these units were delivered to a group at Indiana University. The fast decision module (FDM) contains an ECL-addressable 17- bit fast memory in a single width CAMAC module. This unit, developed for the NSCL 4π Array, provides a rapid mechanism to convert complicated detector hit patterns into multiplicities. We have sold 2 FDM's to a group at SLAC, and LeCroy has expressed some interest in picking up the module. The Fera Faucet-Maier (FFM) is a VME based control module including a deadtime gate developed in close collaboration with Skip Vandermolen and the NSCL 4π group to efficiently read out LeCroy FERA (fast encoding and readout) ADC's and form the data into single event groups. The FFM has been extensively tested and the final circuit board has been ordered.

Several large projects are underway. We are finishing the construction of ten units of a (4x6) fan-in fan-out module. This module was started as a development project and because of its perceived utility was continued into production. It is denser than the commercial (4x4) modules and incorporates, blinking lights to signal valid inputs. As part of the NSCL contribution to the APEX collaboration, we are designing a fast high resolution silicon preamplifier and a 16 channel CAMAC constant fraction discriminator. A working prototype of the preamplifier circuit board has passed all the acceptance tests of the APEX group and we are waiting for the mechanical specifications of the motherboard before final layout. One layout of the CAMAC-CFD was completed but has to be revised because the APEX group significantly changed the specifications of the module.

---

a. Electrical Engineering Department, MSU.

TEST OF A SEPARATED FET PREAMPLIFIER FOR A BRAGG CURVE SPECTROMETER

J. Yurkon, M. Maier, G. Westfall, D. Swan and D. Kataria

We have tested a separated FET preamplifier for use with the Bragg Curve Spectrometer (BCS) of the 4π. We will not show the circuit design here since it has been reported elsewhere.[1] The motivation for the test was to see if we could improve on EMI rejection, and reduce the noise due to cable capacitance, by putting the FET close to the anode of the BCS. This necessitated separating the FET due to the high fraction of solid angle that must be maintained. The FET was placed 15 cm from the preamplifier. The preamp. body was separate from the BCS, while FET, anode, and biasing network was shielded by an electrically conducting layer of aluminum tape. The tape was used to simulated the silver epoxy paint that will shield the production models.

The BCS was tested with 500 torr of P5 gas. It had a 1/3 mil thick aluminized Kapton entrance window. A Th228 source was placed in the position where the target would be normally. The energy spectra is shown in Figure 1. At 500 torr the 8 MeV alphas just range out before the Frisch Grid. The observed widths of the peaks are due primarily to straggling in the 1/3 mil Kapton window. Figure 2 is the Z signal, gated on the 8 MeV alpha line. It shows excellent resolution. The separated FET preamp works well in this configuration and has adequate rise time for the measurement of the Bragg peak.

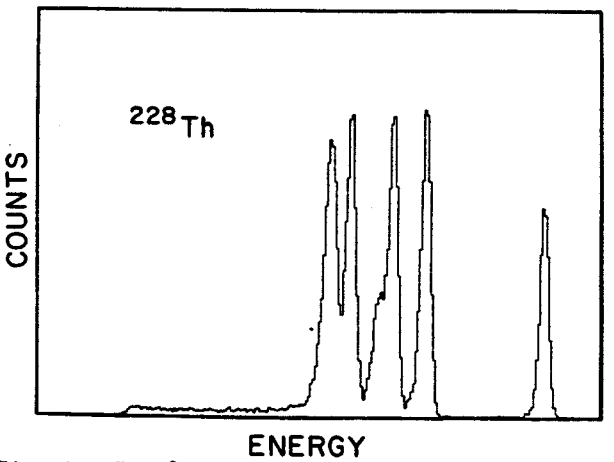

Fig. 1. Th228 Energy Spectrum in BCS

References

1. W.G. Gong et al., Nucl. Inst. & Meth. A268(1988)190.

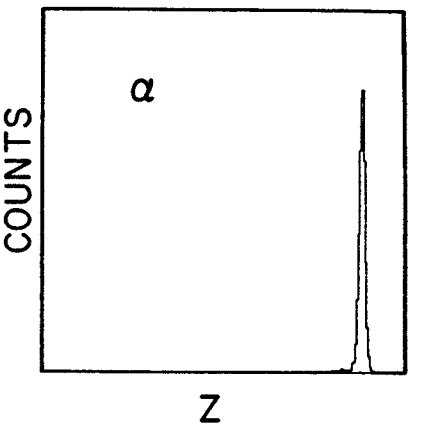

Fig. 2. Th228 8 MeV alpha Z signature.

EXPERIENCES WITH A MOBILE DATA ACQUISITION SYSTEM

R. Fox

Introduction

In last year's annual report, we described the development and early experiences with a new networked data acquisition system. In this report we describe the construction of a mobile version of the system and some early experiences with it.

First we describe why one might wish to construct a mobile system. We next describe what the NSCL mobile acquisition system looks like. Finally we describe initial experiences with the system.

Motivation

There are two reasons why one would like a mobile version of a nuclear data acquisition system. First, it is sometimes the case that funding restrictions do not permit a complete instrumentation of all of the experimental halls. Second, one would like to perform experiments at other laboratories with special requirements.

In the latter case, a mobile acquisition system allows advance set up and testing of programs and hardware at the collaboration's home institution in a hardware and software environment which are identical to the eventual running conditions. Following extensive development and testing at the home institution, the debugged system can be transported to the laboratory where the experiment is scheduled, and run without modification.

In the former case, moving data acquisition systems around from place to place in response to the accelerator schedule allows the a laboratory to operate with fewer data acquisition systems than experimental areas. This enables NSCL to make most cost efficient use of computing resources for data acquisition.

Form of the Mobile System

The NSCL mobile acquisition system is essentially the standard NSCL front end. This system has been describe elsewhere [1], [2]. The system connects to back end computing via ETHERNET. A special purpose data transport protocol is used to send data from the front end to as many back end computers as desired [3]. RS232 connections are used to perform run control, and to send commands to the debugging monitors during program downloads. Readout software itself is loaded into the processors via ETHERNET.

The requirements of the mobile acquisition system front end were as follows:

1. The system had to be easily transportable without disassembly.
2. The system has to be easy to move from place to place. Ideally, a single person should be able to move the front end.
3. For a large fraction of experiments done at NSCL, anyway, the system should be self contained.
4. No software configuration should be required to move the system from place to place.

These goals were accomplished by mounting the following hardware in a relay rack on wheels:

1. The VME card cage containing the front end computer system.
2. Two CAMAC crates.
3. An ETHERNET terminal server running the LAT protocol.

The system was internally pre-cabled so that, in addition to connections required to CAMAC modules for a particular experiment, one

need only supply power, and two ETHERNET transceiver cables to the system to bring it up. The terminal servers in the mobile units are configured as an appropriate mix of standard terminal lines, and outbound (reverse LAT) services to the front end CPUs. As a result, wherever the front end goes, several free terminal lines go as well.

A 'travel hardened' version of the system was also constructed. In that version of the system, the relay rack has mounting rails which allow the front end equipment to be recessed from the rack front sufficiently so that internal cabling does not extend beyond the front of the rack. This allows that system to be boxed and shipped without disassembly.

Experiences with the system

The initial use of the system was for IUCF experiment E301. In that experiment, the front end, in addition to experimental read out, performed local computations on the data which included the computation of a set of derived parameters, and a run time settable gate on the values of those derived parameters which could reject events which did not meet the gate.

The front end code was developed completely at NSCL. A test setup was used to completely debug both front end and back end software prior to the run. In the course of these tests, one of the NSCL computers was made to appear as if it were the computer we would use at IUCF.

Following extensive testing, the system was boxed and trucked down to IUCF. Within 24 hours of arrival, the entire NSCL acquisition system was up and running taking pulser data from the front end.

Conclusions

Experiences with the mobile system have been uniformly favorable both within NSCL and on the one occasion it was taken on the road. The system provides a method for making cost effective use of laboratory resources both on internal and external runs.

References

1. R. Fox, R. Au, A. VanderMolen A Multitasking, Multisinked, Multiprocessor data acquisition front end IEEE Trans on Nucl Sci. V 36 No. 5 pg. 1562
2. R. Fox, R. Au, A. VanderMolen Advances in the NSCL Data Acquisition System. NSCL 1988 Annual Report pg. 88
3. R. Fox, R. Au, A. VanderMolen A network protocol for data acquisition at NSCL IEEE Trans on Nucl. Sci, V 36 No 5 pg. 1608

STATUS OF THE 4 PI DATA ACQUISITION SYSTEM

A. Vander Molen, R. Au, R. Fox, M. Maier and M. Robertson

The data acquisition system for the 4 Pi has been upgraded over the last year to the new labwide MC68020 based system. The system is completely compatable with the labwide system with the exception of the "user" sections of the slave code. This compatability will allow for easier upgrades, maintainence and support.

The slave code has been modified to a larger parameter set. This set, used for CAMAC settings, has been mapped to all available CAMAC slots in the 4 Pi system.

The original design of the data acqusition system called for the use of the LeCroy ECLine bus for data transfers. This bus could lead to transfer rates up to 10 Mbytes/sec. Modules designed and built by Creative Electronics Solution to interface the ECLine and VME were purchased and tested. These modules would transfer data near the 10Mbyte/sec rate to memory accessable to the acquisition system under test conditions. It was found, though, that this system would not allow for definitive event boundaries in the data stream or dead time control.

An interface module, dubbed the FERA FAUCET MAIER, was designed, built and tested to rectify these problems. This module supplies all necessary signals for the ECLine data transfer, deadtime control and clear signals. In addition the module will place a user definable header between each event. A prototype module in a complete 4 Pi setup transfered data to memory at rate around 5 Mbytes/sec. Rates to data storage were constrained to 400 kbytes/sec by the Ethernet. Production boards have been ordered.

STATUS OF THE APEX COLLABORATION

E. Kashy, S. Austin, D. Mikolas, J. Winfield, M. Maier and the APEX Collaboration.

APEX (Atlas Positron Electron Experiment) is an experimental collaboration of researchers from several laboratories. Its goals are the measurement of positrons and electrons produced in heavy ion collisions, using ions near uranium with energies near the coulomb barrier. The member institutions include Argonne National Laboratory, Rochester University, Princeton University, Florida State University, University of Washington, Yale University, and Michigan States University.

The tasks of building, acquiring, and testing the various components are shared among the collaborators. MSU's principal responsibilities currently include the Heavy ion counter array, preamplifier design and construction, design and construction of high density (16/module) constant fraction discriminators, and of peak to FERA converters for analog pulses. MSU also share with ANL the design of the logic involved in the data acquisition system. The status of these parts of the APEX project can be found in the following contributions to this annual report.

Management of the project is done by a steering committee with one representative from each institution. Coordination of the efforts is made by two elected coordinators, one from ANL, and one from another institution. For the July-Dec 89 period, these were Betts (ANL) and Kashy (MSU). For Jan-June 90, Betts (ANL) and Hallin (Princeton), and for July-Dec 90, Betts (ANL) and Wolfs (Rochester)

Description of the experiment:

A target with A near 238, on the axis of a large solenoidal magnetic field of 300 gauss magnitude is bombarded by a beam with similarly high A value, and with energy near 6 MeV/A. Scattered and recoil nuclei are detected in an array of heavy ion PPACs which subtend most of the solid angle from 22 to 68 degrees in the lab. Electrons and positrons produced in the collisions spiral away from the target and are detected by two multi-detector arrays (about 200 on each side) made of silicon PIN junctions.

By timing the flight of electrons and positrons from the target to the silicon detectors, one can reconstruct the angle at which they were emitted from the target. Thus, in a coincident event of electron and positron emission, the mass of the progenitor object which may have given rise to the lepton pair can be obtained. Finally, the identification of positrons in the presence of far more abundant electrons is made by two large NaI detector arrays, arranged in the shape of a cylinder with the Si array on its axis. The two 511 keV photons which result from the annihilation of the positrons provide the necessary positron identification. In addition, the position of the source of these photons can be obtained, as the NaI crystals have position sensitivity.

Figure 1 is a schematic view of the solenoid coils and of the vacuum tank.

Status of various components:

Coil and Chamber: This is being done by the Princeton team. The B-field calculations have

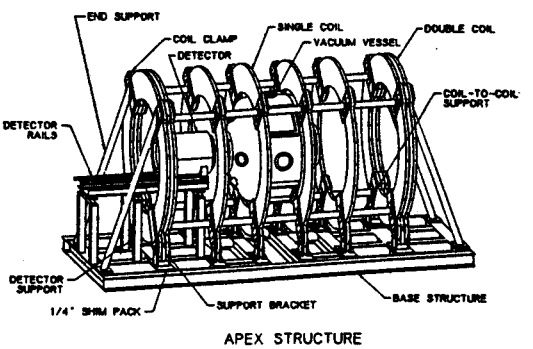

Figure 1. Schematic view of coils and vacuum vessel.

been done and checked and assembly of the coils is progressing. The coils used were provided by MSU to ANL on a loan basis, and were initially used in the now decommissioned K-50 Cyclotron. The chamber design is almost complete, including the required pumping system of this rather large (2.4 cubic meters) apparatus.

NaI Array: Performance of two prototype bars of NaI scintillator have been carried out initially at ANL, and current responsibility for these detectors has been taken over by Yale. Design for the mounting mechanism has been done. Bids for the complete array have been received and a purchase order will be issued soon.

Si detectors: This is a major cost as well as uncertainty item, in view of the exacting performance requirements: An energy resolution near 6 keV and timing width of 2ns, so that both angle of emission and energy of the electrons can be measured. This makes demands on both the PIN junctions and the electronics. Two sets of prototype detectors, 1mm thick, have now been ordered from two different vendors. A single prototype detector, 1mm thick and one centimeter square in area, has been tested with commercial electronics and has met the requirements. Very recently, these have also been met with MSU designed electronics. Tests of the ordered prototypes (each chip has three 0.5x1.5 cm junctions) should be done in the next four months. Procurement of the detectors, as well as the mounting system and testing is being done at ANL. The current mounting scheme includes a thin envelope around the array, within which cooled gas at low pressure is circulated and serves to cool the detectors.

Targets and target holder assembly: Because of the target deterioration which results during the bombardments, this is a significant problem in the investigation. Local changes in target thickness introduce spread and uncertainty in in the bombarding energy, so that if the reported phenomena are resonant in nature, this will make results difficult to reproduce. A rotating target system is being developed at Florida State to minimize these effects. In addition, several measurements of the effect of very low energy beams, but with specific ionizations similar to those expected in the experiments, have been carried out at ANL. These have tested both the initial homogeneity of targets prepared of different compounds and the deterioration of these targets as function of beam intensity and bombardment time.

Beam monitoring detectors: These will monitor the beam position and direction on target throughout the data acquisition process. High resolution ionization chambers are being designed and tested at University of Washington for that purpose.

The status of the experimental information on electron and positrons associated with collisions of heavy ions which has been accumulated over the past few years can be found in a recent (1989) review article (ref.1). Since that time, experimental results from the 'Orange' group at Darmstadt confirm once again the reported narrow peaks in the energy spectrum for the sum of the electron and positron energies when emitted in coincidence (Ref. 2). There is at present little agreement as to the interpretation and origin of these narrow peaks.

References

1. A. Schafer, J. Phys. G: Nucl. Part. Phys. 15, (1989)373-416.
2. E. Berdermann et al. Contribution to the forthcoming 1989 GSI Annual Report.

ELECTRONICS FOR THE APEX COLLABORATION

M.R. Maier, E. Kashy, S. Austin, D. Mikolas and J. Winfield

As part of the APEX collaboration at ANL, an experiment where one looks for very weak positron electron coincidences, NSCL has agreed to build the electronics for the Silicon-detectors.

The task is to construct a pulse-processing chain for 436 Silicon-detectors with "state of the art" resolution. The requirements are energy resolution better than 6 keV FWHM, and time resolution better than 2 nsec FWHM at 300 keV energy. Commercial preamplifiers have been shown to deliver this performance.

We are designing and building a "fast-slow" preamplifier which will deliver a fast output signal for a constant fraction discriminator and an energy signal for a peak to charge converter. This latter unit is necessary because APEX is using charge integrating FERA-digitizers. We are also designing a 16-channel constant fraction discriminator with ECL outputs and current source outputs where the magnitude of the current can be controlled via CAMAC. This should make the time to FERA convertors used in the standard setups obsolete.

The peak to charge converter will also be designed. It will be useful to process the standard slow shaping amplifier outputs, characterized by long rise times and pulse widths - so that they can be used with the FERA ADC's.

All of these projects have been proposed in the past, but this time APEX will come up with the motivation and the funds for development.

The present status is the following: The preamplifiers have gone through several iterations, and we are confident that they will meet the specifications. The constant fraction discriminators layout will be changed to include the new features that the APEX-experiments have requested. Since space is limited in a CAMAC module this is not easy, but by changing some internal I.C.'s it should be possible to squeeze everything onto the PC board.

The peak to charge converter is presently in the early design stages. We will use an implementation proposed by G. Westphal[1], which is used also in the SILENA peak sensing ADC's.

References

1. G.P. Westphal; NIM 115(1974)509.

DEVELOPMENT OF A HEAVY ION DETECTOR ARRAY FOR APEX

D. Mikolas, E. Kashy, D. Kataria, J. Yurkon and the APEX Collaboration

I. Introduction

In all experiments to date which have produced narrow peaks in the positron spectrum from Coulomb-barrier heavy ion collisions, the event trigger requirement has included detection of the scattered nuclei within some angular range. This trigger establishes that the nuclei have come within some tens of fermi. In the proposed APEX experiment an array of heavy ion counters which detects all (high-Z) nuclear products with a scattering angle θ of between roughly 20° and 70° is required. These counters determine the scattering angle and time of flight (TOF) of both coincident nuclei. With the assumption of two-body kinematics this information is sufficient to determine the scattering angle in the center of mass (a measure of distance of closest approach), the reaction Q-value, and the masses of the outgoing particles. The accuracy to which these quantities can be determined is balanced between the energy straggling and multiple scattering of the lower-energy member of the pair, and the resolution of the detectors themselves in velocity (TOF and path length) and scattering angle. Goals consistent with readily achieved resolutions with other detectors and with the unavoidable effect of multiple scattering in the target have been established. For TOF: 0.5ns FWHM; and for θ: 0.15° FWHM.

Sufficient segmentation in ϕ was required to correct for the effect of the weak (300 Gauss) transverse magnetic field of APEX over the roughly 60 cm flight path of the heavy ions, to reduce the count rate in each segment to a value well below 10^5 counts/second for a 10 pnA U beam with E/A = 5.9 MeV (just below the Coulomb barrier) on a 300 $\mu g/cm^2$ U target, and to minimize the capacitance of the detector.

II. Mechanical Strategy

The array consists of eight trapezoidal elements assembled into a truncated right octagonal pyramid. Each element is divided into three electrically isolated heavy ion counters, giving a total segmentation of 24. This geometry was chosen because it closely approximates a cone (best use of space) and it keeps the segmentation high while keeping the total number of parts and of independently sealed gas volumes low. A schematic of the array is shown in Fig. 1. A cross section of the APEX prototype detector element is shown in Fig. 2.

III. Position Read-out

The measurement of the scattering angle of a particle which strikes a given segment can be reduced to a 1 dimensional measurement if the position sensing elements are shaped as conic sections rather than straight lines. Curved electrodes can be etched on copper-clad PC board which serves as both electrode and rear vacuum window. While delay-line read-out of the traces could then be made with commercially packaged lumped constant delay-line devices on the back of the detector connected via plated through holes in the PC board, a more natural solution was chosen. The roughly 500 curved traces on the PC board are connected end-to-end, making one long transmission line with the copper-clad back of the PC board as a ground plane. This has the advantages of smaller and more periodic differential non-linearities than the discrete devices, and adds no additional expense or required space or assembly operations. Further, any shifts in position calibration due to the effect of the magnetic field of APEX on the ferrite core inductors of the discrete delay

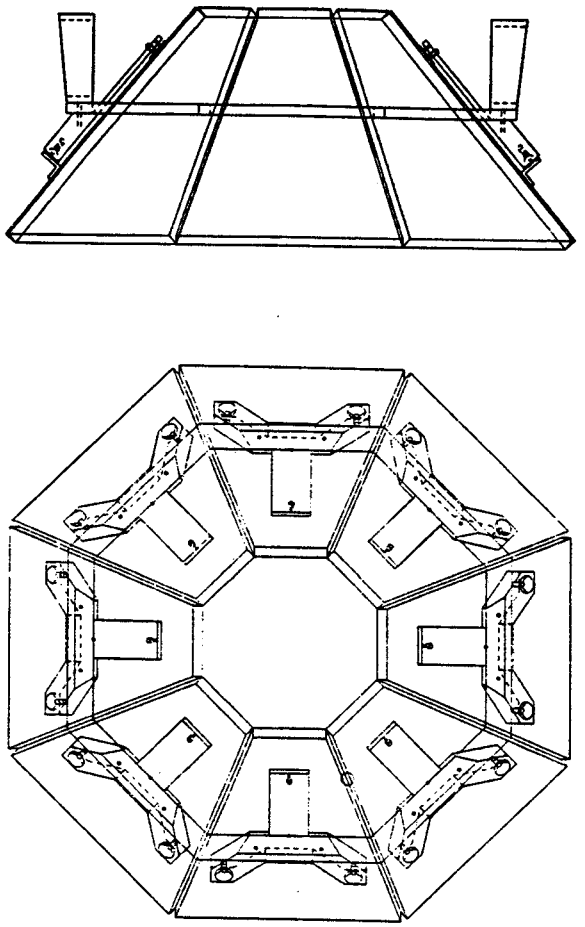

Fig. 1. Schematic of the APEX heavy ion detector array and mounting frame to the exit port of APEX. The eight detectors are supported by eight "T-bars" attached to one octagonal frame.

MSU-90-092

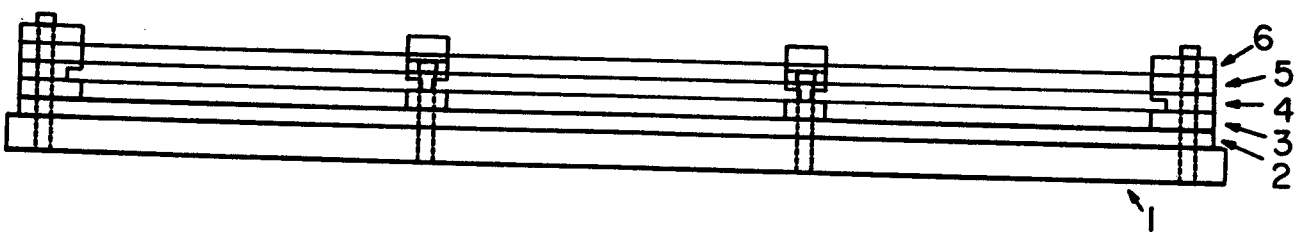

Fig. 2. Cross-sectional view of one APEX detector element. 1) 1/4" thick aluminum or magnesium back plate, 2) 1/64" thick meander PC board, 3) anode plane, 4) front cathode plane, 5) pressure window frame, 6) support wire frame.

lines are avoided. Finally, the minimum delay per trace that would be possible with discrete devices is 1ns (Rhombus Industries Inc.), making the total delay about 500 ns. The average count rate per detector segment is expected to reach 40,000 counts per second under the conditions described in the Introduction. The corresponding average interval between counts is 25 μs, giving a pile-up rate of 2% of the count rate. The shorter overall delay of the meander delay line (roughly 200 ns) is thus preferable.

IV. Front Cathode Frame:

A front cathode foil was added to terminate the electric field lines extending from the anode. An added benefit is the factor of two increase in gain from the additional avalanche.

V. Pressure Window

The role of the pressure window is to maintain the gas volume and insure that no differential pressure occurs across the front cathode foil.

Experience from GSI indicates that Kapton is the best choice as a pressure window material for a heavy ion counter which will be exposed to high radiation levels from the target. Other materials fail and begin to leak detector gas into the vacuum vessel, or fail catastrophically.

VI. Support Wires

In order to support the pressure window against extreme distortions, thin wires (0.004" dia. stainless steel or Be Cu) will be stretched across the inside of the final support wire frame. Wires will be epoxied into thin groves which are slightly larger than the wires themselves.

VII. Meander Delay-line Tests

Preliminary tests of meander delay lines on PC boards indicated that the propagation of signals through the meander sometimes behaves differently from that predicted for a long isolated single trace. Because of this unpredictable behavior, a series of tests on a large set of meanders was carried out to determine absolute delays and impedances, and to attempt to understand the systematics of their behavior. In all, the impedances and delays of 72 meanders were measured. This group consisted of all the permutations generated from a choice of three trace patterns, four PC board thicknesses, two meander widths and three ground-plane geometries. The three trace patterns are referred to by their approximate periods and widths in mm; 1-0.5 (0.039", 0.027"), 1.5-1 (0.059", 0.047") and 2-1 (0.080", 0.046"). The four standard PC board thicknesses used were 1/64", 1/32", 1/16" and 1/8". The two meander widths studied were 1.00" and 1.80". Three ground plane geometries were studied. The first was a simple continuous ground plane (GP), the second, a parallel meander directly below the top trace (PAR), and the third an anti-parallel meander, a mirror image of the parallel meander ground plane (ANTI) (reflected about an axis parallel to the average propagation direction of the signal down the meander.) The copper thickness was 61 mg/cm^2 in all cases. In Fig. 3, a 1-0.5 1.8" wide test meander is shown. The results of these measurements are summarized in Table 1. Both impedance and time delay measurements were made with a Time Domain Reflectometer (Tektronix 1502B Metallic TDR Cable Tester.)

VIII. 4"×4" Detector Tests

First tests on a 4"×4" square MWPC with a meander-type delay line for 1 dimensional position read-out were performed using a ^{252}Cf source, collimated by a series of 1mm slits in 0.001" Al foil. The anode was biased through a 1MΩ resistor, and the anode signal was coupled through a 0.001μF capacitor on the detector.

Electronic characteristics of the meander cathode were determined. The meander was produced on a 0.003 inch thick sheet of Kapton, covered with 0.001 inch of epoxy and 15mg/cm^2 (17μm, 0.7mil) of copper on each side. The meander covers an area 12cm square. The traces are 1mm wide with a period of 2mm. The transmission impedance is 11±2Ω. The DC resistance of the meander trace is 3.5Ω. The total length of the meander is 740cm. When a step is introduced at one end and the other end is left as an open circuit, the 50% point of the

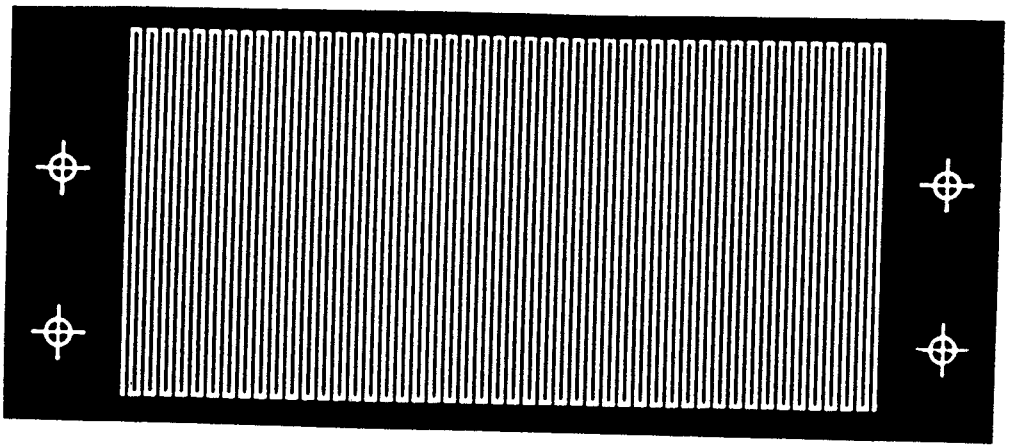

Fig. 3. 1.8" wide 1-0.5 meander pattern.

Table 1. Impedance and speed for various meander patterns, ground plane configurations, and PC board thicknesses. The test setup is described in the text. The first row of values for each delay line type is the impedance (Ohms), and the second row is the dimensionless speed (L/ct).

Meander		1/64"	1/32"	1/16"	1/8"
2-1	GP	35.20	51.50	74.00	105.0
		0.41	0.47	0.63	0.85
1.5-1	GP	33.00	49.50	71.00	100.0
		0.62	0.77	1.10	1.15
1-0.5	GP	51.0	72.5	98.0	140.0
		0.56	0.70	1.00	1.39
2-1	PAR	42.0	68.0	105.0	145.0
		0.38	0.41	0.51	0.85
1.5-1	PAR	41.5	68.0	101.0	140.0
		0.54	0.62	0.84	1.44
1-0.5	PAR	65.5	104.0	140.0	198.0
		0.48	0.55	0.76	1.07
2-1	ANTI	70.5	90.5	114.0	140.0
		0.23	0.31	0.47	0.65
1.5-1	ANTI	60.5	80.5	107.0	140.0
		0.38	0.53	0.81	1.14
1-0.5	ANTI	82.8	110.0	142.0	190.0
		0.38	0.52	0.76	1.07

reflected wave returns 90ns later. This gives L/ct = 0.54. The rise time is then 3.5ns. The meander impedance was matched to the 50Ω coaxial cable with transformers (Minicircuits T4-1).

A position resolution of better than 1.5mm FWHM was obtained, using the mask described above as shown in Fig. 4. The position resolution was the same when timing between the two ends of the meander (600ps FWHM) and between either end of the meander and the anode (300ps FWHM). This suggests that the resolution could be dominated by the slit width or by fluctuations from one avalanche to the next. The timing resolution of the detector was found to be better than 300 ps for small areas.

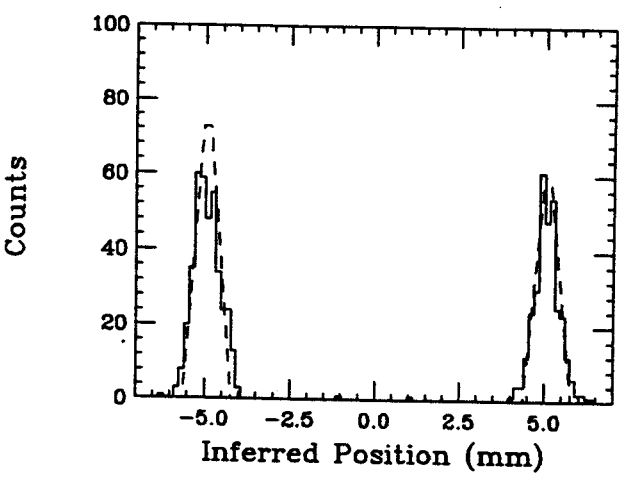

Fig. 4. Results of position resolution test.

APEX DATA ACQUISITION SYSTEM

J.S. Winfield for the APEX Collaboration[a]

The APEX detector falls into the "Large" category as far as nuclear physics experiments go. There will be 432 channels each of energy and timing from the silicon arrays, 96 channels each of energy and timing from the NaI detectors, and 72 channels of timing from the heavy-ion counters. In view of this, it is essential that the data acquisition system be based on low-cost-per-channel modules and incorporate zero suppression of the data.

For the energy signals, the LeCroy 4300 series CAMAC FERA system was chosen. We originally considered the LeCroy 4290 series for the timing channels because it would give a lower cost per channel compared with the less densely packed FERA system. The LeCroy 4291B TDC was evaluated at Argonne National Laboratory by Frank Wolfs after factory modification of the resolution to 250 ps/channel. The system was found to be very sensitive to temperature fluctuations and had poor long term stability. Variations of as much as 750 ps were observed in the centroid. However, the TDCs can be automatically re-calibrated by the AUTOTRIM feature. With an hourly execution of the AUTOTRIM cycle, the time peak fluctuations were kept to within ±1 channel, or ±250 ps, but attempts to improve further the long-term stability were unsuccessful. Such drifts are acceptable for the silicon detectors (resolution = 1.5 ns) and the NaI detectors, but not for the heavy-ion counters (resolution = 500 ps).

For the above reason, as well as the advantage of compatible data encoding (discussed below), the FERA system was chosen for the timing as well as the energy channels. This became economically feasible once the time-to-charge converters were incorporated into the NSCL 16-channel CFD's (see contribution on APEX electronics elsewhere in this report).

The readout of the FERA's will be done via ECL-bus (as done with the present MSU 4π Array acquisition system). An all-FERA system has the advantage that the energy and time signal layout can be done in a parallel fashion. Then an energy-time coincidence requirement for a given

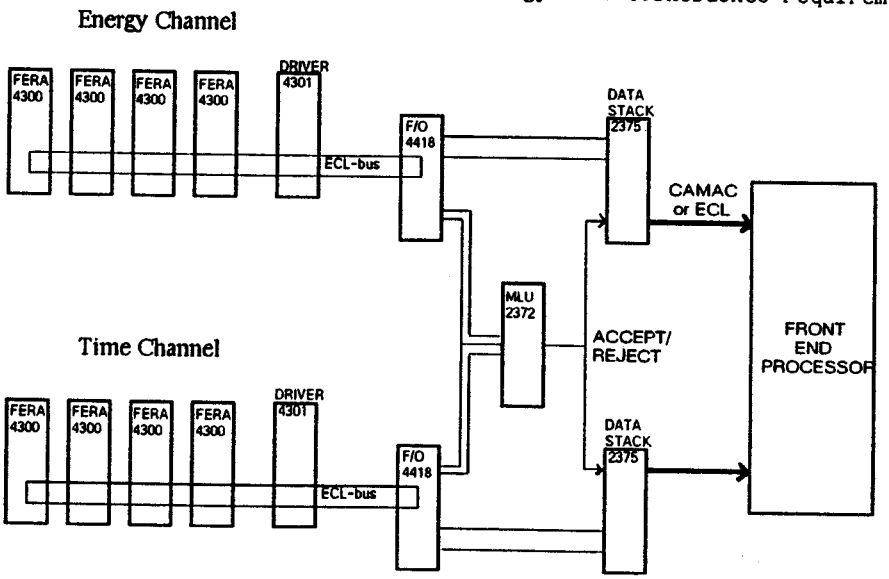

Fig. 1. Schematic layout of the proposed energy and time matching for the silicon detector data. The FERAs are read in zero-suppressed mode. The memory lookup unit (MLU) checks for a matching time word for each energy word in a given event.

silicon detector can be made very conveniently in ECL-logic with CAMAC memory lookup units (i.e. before the data acquisition computer is triggered). The valid data (data for which there is both an energy and time signal) will be stored in a CAMAC data stack before being processed by the front end computer. The flow of data is illustrated schematically in Fig. 1. A similar system to the one proposed for APEX has been developed for the TASCC (Chalk River) 8π spectrometer.[1]

The NSCL MASH system[2] is being considered for the APEX data acquisition front end. The existing Argonne DAPHNE system has the disadvantage that it uses a non-commercial event handler which is no longer available.

---

a. Argonne National Laboratory, Florida State, Michigan State, Princeton, and Rochester universities, University of Washington, and Yale University.

References

1. J.P. Martin et al., Nucl. Instr. Methods, A257, 301 (1987).
2. R. Fox, R. Au, and A. VanderMolen, IEEE Trans. Nucl. Sci. NS-36, 1608 (1989); see also contribution elsewhere in this report.

A BRAZING FURNACE FACILITY AT NSCL

D. P. Sanderson, J. Nolen Jr., S. Hickson and J. Yurkon

A facility is under construction at NSCL for brazing and metallizing ceramic insulators. The facility is needed to quickly develop custom ceramic-metal assemblies for the cyclotrons. RF couplers and deflector assemblies are two examples.

The furnace consists of a vacuum vessel with a cylindrical resistive heating element. (See Fig. 1.) Solid state relays, switched by a computer operated temperature controller, feed power from a three phase 480 volt variac to a 32:1 step down transformer providing up to 2300 amps of current to the elements. Heat shielding is provided by four layers of tungsten sheet and three layers of molybdenum. The hot zone is 22.9 cm in diameter and 30.5 cm long. Pumping is provided by a 15.24 cm diameter diffusion pump with a liquid nitrogen trap. The use of polyphenyl ether diffusion pump fluid should reduce backstreaming to undetectable levels. Water cooled feed throughs are used for power. The temperature of a part is monitored using a tungsten/5%rhenium-tungsten/25%rhenium thermocouple and an optical pyrometer. The vessel is a large multiport stainless steel chamber with cooling lines brazed to the outer shell. For operations requiring a reducing atmosphere, a standard laboratory detector gas handling system can be used to continuously flow a mixture of nitrogen and hydrogen through the system.

The furnace is housed in its own laboratory next to the south hallway. The room will include an air furnace as well as diagnostic equipment for examining brazed assemblies.

Three ceramic-metal joining processes are presently being carried out in a small version of this furnace in the detector laboratory. Ceramics are first metallized with a tungsten

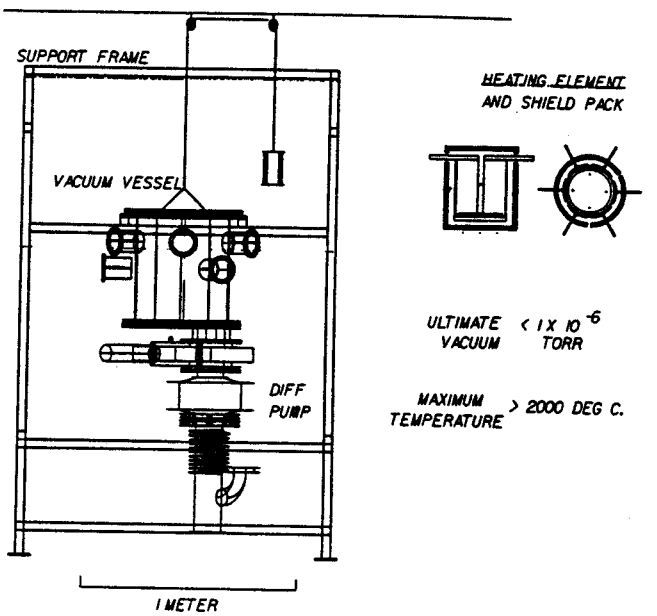

Fig. 1. The brazing furnace.

slurry in a reducing atmosphere. The metal is nickel plated in an electroplating bath and then brazed to its assembly in the small furnace. We will be able to carry out all of these processes in the new facility. With the high vacuum available from the pumping system, we will try an active metal brazing process in which titanium in the brazing alloy reacts with the ceramic to produce a tight bond. If this process is as reliable as the three step method, it will greatly shorten and simplify the brazing process.

In summary, the new vacuum brazing facility at NSCL will provide a new tool for custom ceramic assemblies for the laboratory. By shortening the time from design to prototype, their development should procede at an accelerated pace.

HEAVY GASES, ISO-OCTANE AND C_3F_8, IN CHARGED PARTICLE DETECTORS

E. Norbeck[a], J.X. Zhang[a], R. Dayras[b], C. Mazur[b], E.C. Pollacco[b] and D. Swan

In many applications, the usefulness of a gas detector is limited by the amount of gas that it can contain. This is particularly true when the detector is operated in a vacuum and the particles to be measured must be brought in through a thin window. If the gas in a detector is replaced by a gas with the same properties but a higher molecular weight, the same performance can be achieved at a lower pressure. We find that in low-pressure avalanche detectors, iso-octane gives the same performance at 3.0 Torr as isobutane at 5.0 Torr. In low-pressure ion chambers C_3F_6 behaves like CF_4 at more than twice the pressure.

Low-pressure multiwire proportional counters and parallel plate avalanche counters are widely employed as accurate timing and localization devices in heavy-ion research and in a growing variety of other applications. Isobutane is often the gas used in these detectors. Iso-octane, which is two connected isobutane molecules, has almost twice the molecular weight, 114 vs 58 for isobutane. Iso-octane (trimethyl-2,2,4 pentane) is the heaviest saturated hydrocarbon that has adequate vapor pressure and that is readily available as a chemical reagent. It is produced on a large scale as the "100 octane" motor fuel. Because of its multiple branches, this 8-carbon compound has almost the same boiling point (99° C) and vapor pressures as the straight-chain 7-carbon compound, n-heptane, the "0-octane" motor fuel. At 21° C the vapor pressure of iso-octane is 40.6 Torr. Because iso-octane is a liquid, it is much less of a fire hazard than the gaseous isobutane.

The use of the liquid iso-octane requires special techniques when it is used with the usual gas-handling systems. Because the vapor pressure is only 40 Torr, it is essential that there be no small leaks that will allow air to enter the lines between the iso-octane container and the gas handler. The iso-octane container should not be allowed to become warmer than the gas handler or the connecting piping. If it does, liquid will collect at the cooler points.

The iso-octane in the reagent bottle must be transferred to a container that can be attached to the gas handling system. We put the iso-octane in a 10 cm diameter cylinder with a valve on top. After the cylinder was evacuated and the valve closed, a funnel was temporarily attached to the top. Liquid poured into the funnel was drawn into the cylinder when the valve was opened. Any air inadvertently admitted into the cylinder must be removed to prevent the detector from sparking even at a reduced voltage. Air can be removed by pumping directly on the cylinder for an hour or two, however considerable iso-octane collects in the pump oil. The oil can be restored by running the pump for 24 hours with the gas ballast open. A negligible amount of iso-octane is lost from the cylinder if it is cooled with dry ice. (The temperature of dry ice is -80° C and the melting point of iso-octane is -107° C.) There were no problems with the mechanical pump of the gas handler becoming contaminated with iso-octane. The small amount of air that was dissolved in the reagent did not affect the operation of the detector. Pumping for 24 hours at -80° C, which appeared to remove most of the dissolved air, did not significantly change either the pulse height or the sparking voltage. We did not try to remove water from the iso-octane. The label on the bottle of HPLC grade that we used claimed less than 0.01% water.

The resolution of a detector consisting of two parallel plates separated by 3 mm was determined for ^{248}Cf fission fragments. With

iso-octane, the best resolution was obtained at pressures near 3.0 Torr and voltages near 500 V, about 50 Volts below the voltage at which sparking occurred. The pulse-height spectrum showed a peak with a full width at half maximum of 20% of the average pulse height. With isobutane the same resolution could be obtained only at 5 Torr and almost 700 V. The pulse heights were a strong function of voltage and pressure, but under the conditions that gave the best resolution, the pulse heights with iso-octane were only a little larger than those with isobutane. Under these conditions the rise times for the two gasses were the same, about 3 ns. Similar results were obtained with multiwire proportional counters operating in the avalanche mode.

Of the many gases that are used in ion chambers, CF_4 has the advantage of large molecular weight, 88, and fast electron-collection time. It is also non-toxic and will not burn. The heavier fluorocarbons have similar properties and even larger molecular weights. We report here on C_3F_8 which has a molecular weight of 188. It is a gas, the vapor pressure is 6.64 bar at 15°C, and it is available from some of the same firms that supply CF_4. It is important, however, that the gasses be pure. The gasses used here were certified as better than 99.9% pure. One part per thousand of some of the impurities commonly found in fluorocarbons can seriously degrade the performance of the gas in a detector.

The tests were made in a gridded ion chamber[1] that was 55 mm deep with the electric field parallel to the incoming particle direction. A radioactive source supplied alpha particles of 6.06 MeV and 8.78 MeV. A solid-state detector measured the remaining energy of the particles.

The pulse height spectrum from the ion chamber filled with 40.3 Torr of CF_4 was identical to the specrum when the ion chamber was filled with 19 Torr of C_3F_8. When the chamber was filled to 40.3 Torr of C_3F_8, the ratios of the pulse heights in the two gasses were identical to the ratios of the energy losses in the gas as determined with the solid-state detector. It is known that negative ions are formed more readily as the molecular weight of the fluorocarbon increases[2], but under the conditions of these measurements, the number of electrons lost by this mechanism was not enough to affect the operation of the detector.

In conclusion, gas detectors can be operated at lower pressures if the filling gas has a larger molecular weight. The use of iso-octane vapors instead of the highly inflamable isobutane gas entails some change in operating procedure. We do not have any information on the differences in the aging of the detectors with the two gasses.

In the applications studied here, the heavier fluorocarbon gave identical results at less than half the pressure. We have no information about the electron collection time in C_3F_8, except that it was sufficiently fast that electronics designed to be used with CF_4 could be used without change. Our measurements showed no evidence for a reduction in output signal caused by the formation of negative ions, however such a reduction can be expected at sufficiently large gas pressures and drift distances.

---

a. University of Iowa, Iowa City, IA 52242
b. D.Ph.N./B.E., CEN Saclay, F-91191 Cedex, France

References

1. R. Dayras et al. Compte rendu d'Activite du DPh-N, CEN Saclay (1988-1989) Note DPhN/90-1, p.68.
2. L. G. Christophorou, Electron-Molecule Interactions and Their Applications, Vol. 2 (Academic Press, 1984) p. 374.

ENERGETIC (GeV) LIGHT-ION PRODUCTION IN HI REACTIONS

F.D. Becchetti[a], D. Roberts[a], J. Janecke[a], J. Brown[a], K. Ashktorab[a], W. Liu[a], A. Nadasen[b], Z. Yin[c], D. Shen[c]

Measurements of p,α and other LIs produced in the interaction of 85 MeV/u ^{20}Ne stopped in Ta and other targets have been completed. An array of ΔE(Si) and high-stopping power E-BGO scintillators was utilized. The latter were supplied as part of a NSF US-China research program. Spectra (θ - 0°) are displayed in Fig. 1 and deduced moving source temperatures are shown in Table I and compared with our earlier measurements (S. Shaheen, U. Michigan, Ph.D. thesis and submitted for publication). Additional experiments have been proposed at MSU-NSCL using ^{16}O, ^{22}Ne and ^{40}Ar E/A - 85 MeV/u. Two more ΔE(Si) - E(BGO) telescopes will be added for these measurements if approved.

a. University of Michigan, Ann arbor
b. University of Michigan, Dearborn
c. Shanghai Institute of Ceramics, Peoples Republic of China

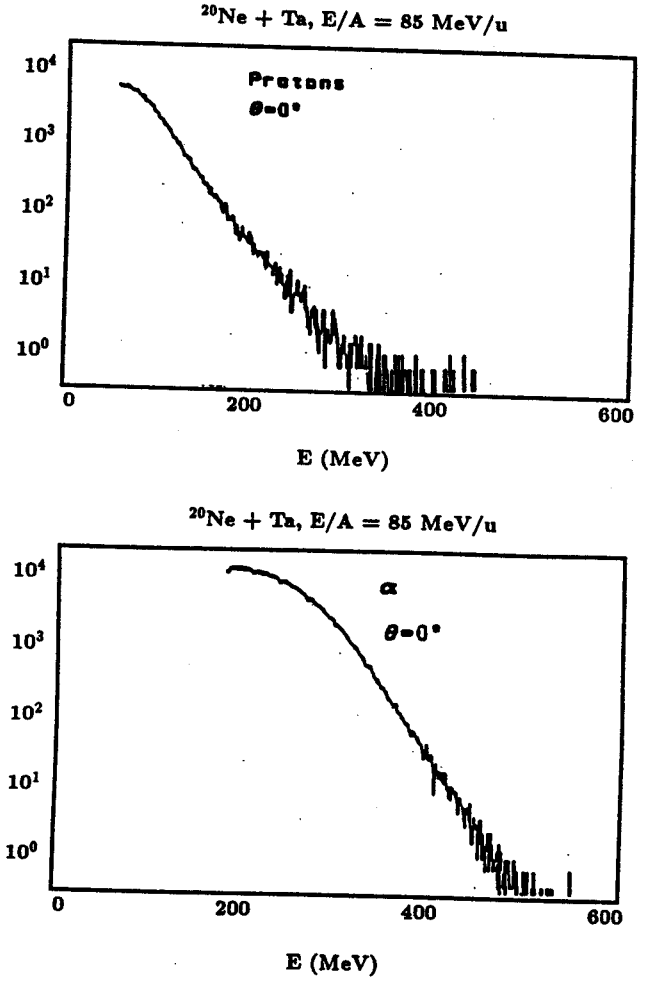

Fig. 1. (^{20}Ne,p) and (^{20}Ne,α) spectra observed for E/A = 85 MeV/u at θ = 0° on a stopping Ta target.

TABLE I

System	*E* (MeV)	*E/A* MeV/u	Protons T_L (MeV)	Protons T_s (MeV)	Alphas T_L (MeV)	Alphas T_s (MeV)
^{32}S + ^{181}Ta	305	9.5	6.4	4.4	12	7
	450	14	11	7.3	19	10
^{58}Ni + ^{181}Ta	600	10.3	5.2	4.2	11	6
^{10}O + ^{181}Ta	480	30	12	7.7	24	14
	640	40	15	9.5	28	17
^{40}Ar + ^{181}Ta	800	20	8.4	5.5	12	7
	1200	30	16	10.4	25	15
^{20}Ne + Ta	1700	85	35.6	23.1	31.2	21.2

7T SUPERCONDUCTING SOLENOID CONSTRUCTION

F.D. Becchetti[a], J. Brown[a], W.Z. Liu[a], D.A. Roberts[a], J. Nolen and A. Zeller

As part of a DoE instrumentation grant a 40 cm bore, 1 m long 7T s.c. solenoid has been designed (Figs. 1 and 2) and initial construction started. The magnet is scheduled for final testing and delivery to MSU-NSCL late summer/fall 1990. It will then be incorporated as part of our radioactive nuclear beam (RNB) research - initially using ^{6}He Beams and $^{18}F^{m}$ or other isomeric nuclei. The device can also serve as a large solid angle reaction product spectrometer for measurement near $\theta = 0°$ (Fig 2)

Another type of use envisaged is as a β^{+}/β^{-} or π^{+}/π^{-} pair spectrometer, e.g. for detection of delepton production or HE γ-rays in HI reactions. A prototype experiment using an existing smaller (3.5T) solenoid has been proposed at MSU-NSCL.

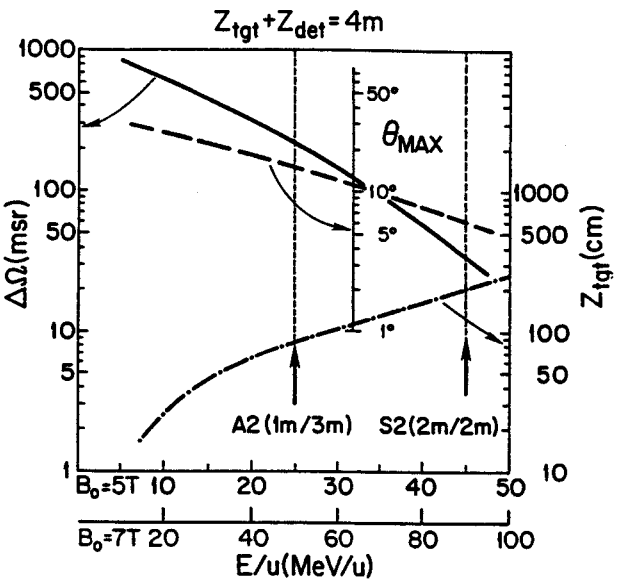

Fig. 2. Capabilities of superconducting solenoid running at B = 5T and 7T for various target/detector, i.e. object/image, positions.

---

a. University of Michigan, Ann Arbor

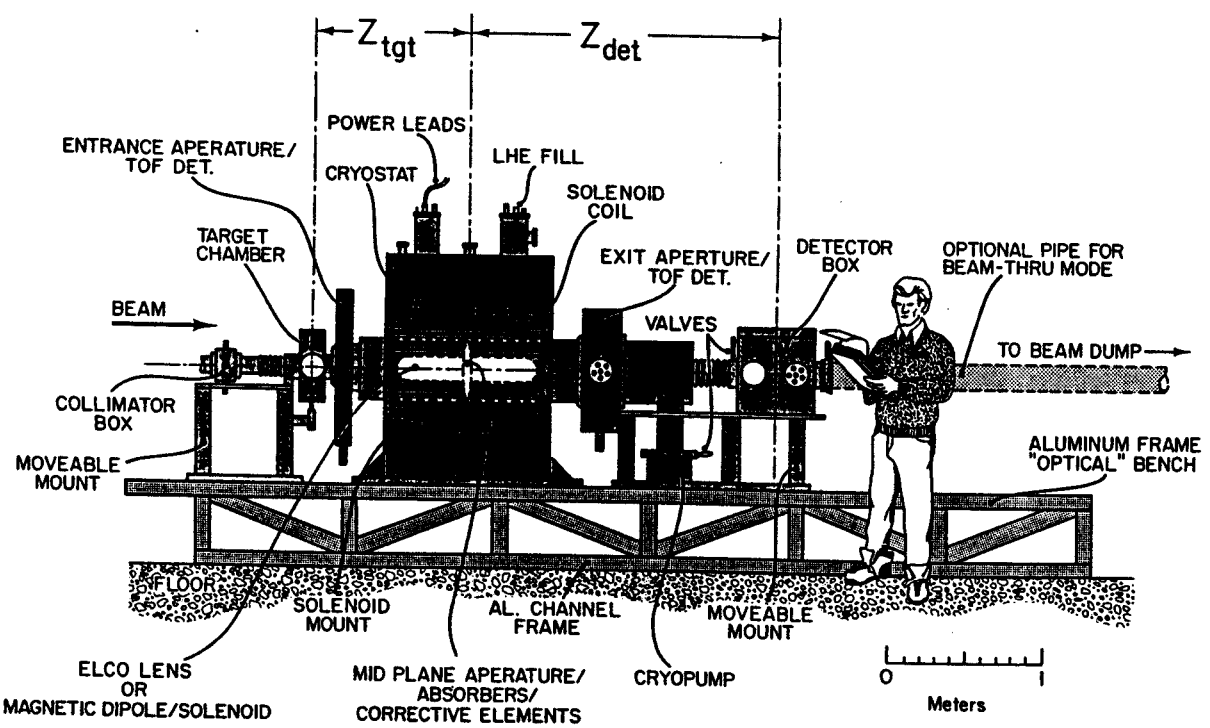

Fig. 1. Layout of 7T superconducting solenoid reaction product collector/spectrometer.